

A Differentiable Sparse Vector Quantization (SVQ) for Spatio-Temporal Forecasting

Chao Chen^{*1} Tian Zhou^{*2} YanJun Zhao² Hui Liu¹ Liang Sun² Rong Jin^{2,3}

Abstract

Spatio-temporal forecasting, pivotal in numerous fields, hinges on the delicate equilibrium between isolating nuanced patterns and sifting out noise. To tackle this, we introduce Sparse Regression-based Vector Quantization (SVQ), a novel technique that leverages sparse regression for succinct representation, an approach theoretically and practically favored over classical clustering-based vector quantization methods. This approach preserves critical details from the original vectors using a regression model while filtering out noise via sparse design. Moreover, we approximate the sparse regression process using a blend of a two-layer MLP and an extensive codebook. This approach not only substantially cuts down on computational costs but also grants SVQ differentiability and training simplicity, resulting in a notable enhancement of performance. Our empirical studies on five spatial-temporal benchmark datasets demonstrate that SVQ achieves state-of-the-art results. Specifically, on the WeatherBench-S temperature dataset, SVQ improves the top baseline by 7.9%. In video prediction benchmarks—Human3.6M, KTH, and KittiCaltech—it reduces MAE by an average of 9.4% and improves image quality by 17.3% (LPIPS). Code is publicly available at <https://anonymous.4open.science/r/SVQ-Forecasting>.

1. Introduction

Spatio-temporal forecasting (Wang et al., 2022a) has board applications in many domains including environment, climate, transportation, etc. Many traditional methods relying on feature engineering have been studied in the past several decades. Recently, deep learning models are becoming

^{*}Equal contribution ¹Central South University, China ²Alibaba Group ³The author now works at Meta Platforms, Inc. Correspondence to: Tian Zhou <tian.zt@alibaba-inc.com>, Rong Jin <rongjinemail@gmail.com>.

more popular (Wang et al., 2022a). However, as more applications (e.g., weather forecasting) arise, it calls for deep models to accurately predict future dynamics with precise spatial and temporal resolutions.

Despite the various forms of spatio-temporal forecasting approaches, such as the use of graph neural network (GNN) models for unevenly resolved data, our work concentrates on grid-based datasets, one of the most widely adopted structures in the field. Within this context, we address a primary challenge: how to finely balance the preservation of important details against the need to filter out irrelevant noise, thereby enhancing the generalized performance of forecasting models. Although vector quantization (VQ) is effective in reducing noises by constraining latent patterns to a clustered codebook, it is usually limited in preserving the diversity of input patterns, making it suboptimal for spatial-temporal forecasting. We performed a comprehensive suite of experiments, the results of which indicate that, contrary to expectations, nearly all sota VQ methods we examined did not enhance the accuracy of a basic weather forecasting model as shown in Table 4. This outcome may provide insight into the infrequent application of VQ techniques in spatial-temporal prediction tasks.

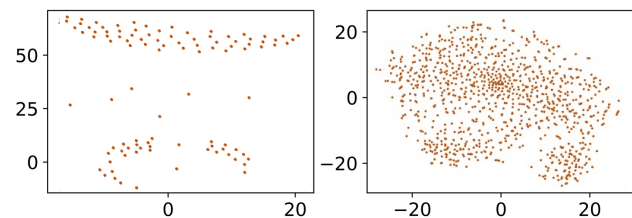


Figure 1. Codebook visualization using t-SNE. Left: VQ updated by k-means clustering and exponential moving average as described in (van den Oord et al., 2017). Right: SVQ with randomly initialized, frozen or learnable codebook. Two methods are trained on WeatherBench-S temperature dataset with the same codebook size (1024).

To address this limitation of VQ, we propose a Sparse regression-based Vector Quantization (SVQ) method. By associating each vector to multiple codes from a large code-

book, it is able to cover diverse visual patterns; by introducing a sparse regularization mechanism in the regression model, we effectively filter out noise and thus ensure a good generalized performance. As shown in Figure 1, our proposed SVQ method exhibits a more uniform distribution of quantized vectors compared to VQ, indicating that SVQ is able to preserve more diverse and fine-grained information from the original inputs than VQ.

Despite employing a series of vectors for representation instead of a single codebook vector, regression-based vector quantization remains true to the foundational aspects of the technique. It still quantizes input vectors into a finite set of discrete levels, utilizing a dynamic codebook-like structure. The key process of mapping input data to representative vectors is maintained, but with the added sophistication of regression models that adaptively combine vectors for a more accurate representation. This method preserves the essence of vector quantization—efficiently compressing and approximating data—while enhancing its ability to capture complex patterns within the input space.

To address the high computational cost of sparse regression, which scales quadratically with codebook size, we approximate the sparse regression model with a MLP model and a large codebook. It not only dramatically simplifies the computation, but more importantly, makes SVQ differentiable and thus easy to train. We emphasize the importance of differentiability of SVQ for its success in spatial-temporal forecasting. Our experiments reveal that lookup-based VQ methods can substantially increase prediction error, despite some employing a residual design that theoretically should perform on par with or better than non-VQ cases. This suggests the “straight-through” estimator, a non-differentiable component of VQ, may be a major factor behind VQ’s underperformance. In particular, the non-differentiable operator such as argmin or lookup introduces errors into gradient estimation of all modules preceding the quantization module, consequently undermining prediction accuracy. In contrast, our proposed SVQ is differentiable and easy to compute accurate gradients for training. We finally note that SVQ also differs from traditional VQ methods by not relying on intricate models to construct the prior distribution of codes, such as the GPT-style model in VQGAN (Esser et al., 2021) or the BERT-style model in MaskGIT (Chang et al., 2022).

Besides differentiability, there are two interesting properties of the proposed SVQ scheme. First, according to our empirical study, we find that with large enough codebook size, we can freeze the randomly initialized codebook without sacrificing any performance, making SVQ potentially more efficient for training. Secondly, unlike lookup-based methods, SVQ allows for both positive and negative weights, enhancing the ability to add or subtract patterns to improve representational power.

Finally, despite its simplification, our experiments across multiple real-world benchmark datasets—including weather forecasting, traffic flow prediction, and video forecasting, demonstrate the superior performance of our SVQ method. In WeatherBench-S temperature forecasting benchmark, it improves the prior SOTA method by 7.9%. For video prediction across renowned datasets—Human3.6M, KTH, and KittiCaltech—SVQ not only achieves a consistent 9.4% reduction in MAE but also enhances perceptual quality, evidenced by a 17.3% lower LPIPS score. These results highlight SVQ’s versatility and superior accuracy in diverse spatial-temporal prediction scenarios.

2. Related Work

2.1. Recurrent-based forecasting model

The majority of spatio-temporal forecasting models leverage techniques such as Conv2D (Xu et al., 2018), Conv3D (Wang et al., 2019a), and attention (Liu et al., 2022b) for spatial modeling. Distinctions among these models primarily arise from how they incorporate temporal information. Recurrent-based models, exemplified by ConvLSTM (SHI et al., 2015), have been widely used to capture motion dynamics by iteratively processing multi-frame predictions. Variants like PredRNN (Wang et al., 2017) introduce the Spatio-Temporal LSTM (ST-LSTM) unit, integrating spatial appearances and temporal variations within a single memory pool. Further advancements include PredRNN++ (Wang et al., 2018) and PredRNNv2 (Wang et al., 2022b), which deepen the model and expand the receptive field through a cascading LSTM mechanism and a memory decoupling strategy, respectively.

2.2. Non-recurrent forecasting model

Despite the effectiveness of recurrent-based methods, they suffer from high computational cost caused by their inherent unparallelizable architecture. Recent efforts in spatio-temporal forecasting have shifted towards non-recurrent models that decouple the forecasting task from autoregressive processes. Notably, SimVPv1 (Gao et al., 2022) and SimVPv2 (Tan et al., 2022) separate spatial and temporal learning into distinct phases within an encoder-translator-decoder structure, consistently surpassing recurrent counterparts in video prediction tasks. Due to their similar architectures, we will collectively refer to them as the SimVP model in the remainder of our paper. TAU (Tan et al., 2023a) refines the architecture by incorporating a visual attention mechanism into the translator. OpenSTL (Tan et al., 2023b) further enhances the translator by MetaFormers.

2.3. Vector quantization and sparse coding

Instead of using continuous latent, VQVAE (van den Oord et al., 2017), a seminal work, integrates vector quantization (VQ) in learning discrete latent representations, typically assigning each vector to the nearest code in a codebook. Subsequent enhancements include Residual VQ (Zeghidour et al., 2022), which quantizes the residuals recursively, and Multi-headed VQ (Mama et al., 2021b), which adopts multiple heads for each vector. While effective, these methods often rely on a relatively small number of codes for representing continuous vectors. Addressing this, SCVAE (Xiao et al., 2023) employs sparse coding, allowing vectors to be represented through sparse linear combinations of multiple codes and achieving end-to-end training via the Learnable Iterative Shrinkage Thresholding Algorithm (LISTA) (Gregor & LeCun, 2010). However, a significant drawback of the sparse coding method using LISTA (dubbed SVQ-raw here) is its high computational complexity, which scales quadratically with codebook size.

Our work is closely related to a simultaneous research work (Tschannen et al., 2023), which employs an infinite cookbook with a linear layer for continuous vector quantization applied in image generation. Despite the similarity, our approach is largely inspired by sparse regression, which is clearly evidenced by our analysis. In particular, we provide a better theoretical foundation and address the challenges arising from spatio-temporal forecasting well.

3. Sparse Vector Quantization (SVQ)

In this section, we will first describe the mathematical foundation for sparse vector quantization, followed by the description of detailed implementation.

3.1. Vector quantization by sparse regression

Let $\{z_i \in \mathbb{R}^d\}_{i=1}^m$ be the set of codes. A typical vector quantization method assigns a data point $x \in \mathbb{R}^d$ to the nearest code in $\{z_i\}_{i=1}^m$. The main problem with such an approach is that a significant part of the information in x will be lost due to quantization. Sparse regression turns the code assignment problem into an optimization problem

$$w = \arg \min_{w \in \mathbb{R}_+^m} \frac{1}{2} \left\| x - \sum_{i=1}^m w_i z_i \right\|^2 + \lambda |w|_1, \quad (1)$$

where $w = (w_1, \dots, w_m) \in \mathbb{R}_+^m$ is the weight for combining codes $\{z_i\}_{i=1}^m$ to approximate x . By introducing L_1 regularizer in the optimization problem, we effectively enforce x to be associated with a small number of codes. Compared to classic VQ methods where codes have to be learned through clustering, according to (Chiu et al., 2022), it is sufficient to use randomly sampled vectors as codes as long as its number is large enough, thus avoiding the need

of computing and adjusting codes. The theoretical guarantee of sparse regression is closely related to the property of subspace clustering, as revealed in Theorem 4.1.

As shown in Figure 2, the obvious downside of sparse regression for VQ is its high computational cost, as it needs to solve the optimization problem in (1) for EVERY data point. Below, we will show that sparse regression can be approximated by a two-layer MLP and a randomly fixed or learnable matrix, making it computationally attractive.

To solve the optimization problem (1), we consider the composite optimization method whose iteration is given as follows

$$\begin{aligned} w'_{t+1} &= w_t - \eta Z^\top (Z w_t - x), \\ [w'_{t+1}]_i &= \text{sgn}([w'_{t+1}]_i) (|[w'_{t+1}]_i| - \lambda \eta)_+, \end{aligned}$$

where $Z = (z_1, \dots, z_m)$, $[z]_i$ is the i th element of vector z , and $(a)_+$ outputs 0 if $a < 0$ and a otherwise. We consider the first step of the iteration where $w_0 = 0$ and have $w = \eta \text{sgn}(Z^\top x - \lambda \mathbf{1}) [Z^\top x - \lambda \mathbf{1}]_+ = \eta \text{sgn}(Z^\top x - \lambda) \sigma(Z^\top x - \lambda)$ and the resulting output for x is given as

$$x' = \sum_{i=1}^m w_i z_i = \eta Z \text{sgn}(Z^\top x - \lambda) \sigma(Z^\top x - \lambda).$$

By generalizing ηZ into another matrix B , we have output vector x' exactly expressed as a matrix and a two-layer MLP over x . We finally note that although it is convenient to form the codebook by randomly sampling vectors, we found empirically that tuning codebook does bring slight additional gains in some cases.

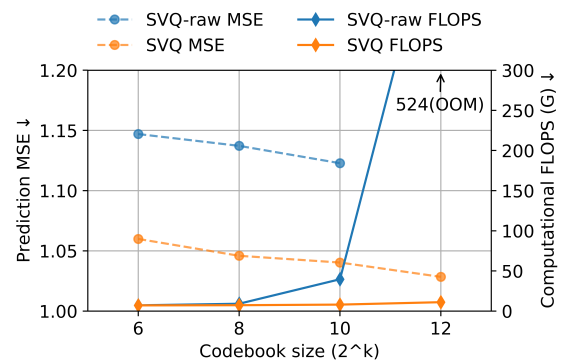


Figure 2. **Effect of SVQ approximation:** Computational cost (FLOPS) and prediction error (MSE) on WeatherBench-S temperature dataset with SVQ-raw and SVQ. The computational complexity of SVQ-raw increases quadratically with the size of codebook, making it suffer from out-of-memory (OOM) issue when scaling codebook size up to 2^{12} .

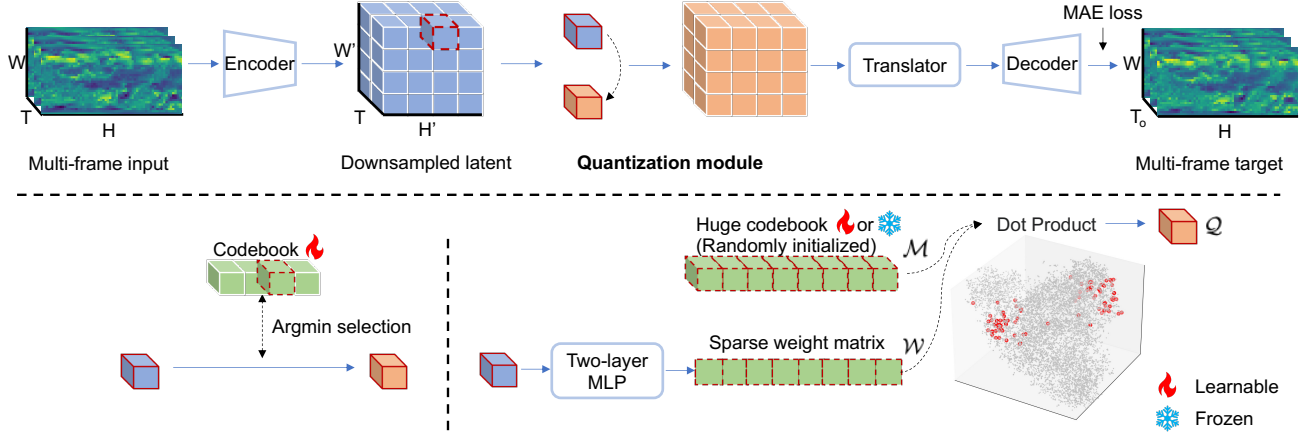


Figure 3. **Top: Architecture of backbone model and the proposed quantization module.** The encoder, translator, decoder are inherited from SimVP. A quantization module is added between the encoder and translator to effectively ensure a good generalized performance. **Bottom: Quantization process of classic VQ (Left) and our proposed SVQ (Right).** In contrast, SVQ select multiple codes (red dots) from a huge codebook (gray dots), and the codebook can be either learnable or frozen.

3.2. Detailed implementation

Architecture of backbone model. As depicted in Figure 3, we adopt SimVP as our backbone model, which encompasses an encoder for spatial feature extraction, a translator for temporal dependency learning, and a decoder for frame reconstruction. We integrate the quantization module between the encoder and translator. The input data is a 4D tensor $X \in \mathbb{R}^{H \times W \times T \times C}$, representing height (H), width (W), time steps (T), and channels (C). The encoder En condenses X into downsampled latent representation $\text{En}(X) \in \mathbb{R}^{H' \times W' \times T \times C'}$, maintaining temporal dimensionality while altering spatial and channel dimensions. This latent space, composed of $H' \times W' \times T$ tokens, each a C' -dimensional vector, undergoes vector quantization.

Quantization module. SVQ comprises a two-layer MLP and a huge codebook. The codebook is a randomly initialized matrix $\mathcal{M} \in \mathbb{R}^{N \times C'}$, where N denotes the size of codebook. To achieve automatic selection of codes, we generate a weight matrix $\mathcal{W} \in \mathbb{R}^{H' \times W' \times T \times N}$ by nonlinear projection from latent representation $\text{En}(X)$. This projection is formally expressed as $\mathcal{W} = \text{MLP}(\text{En}(X))$, wherein the MLP comprises two linear layers and an intermediate ReLU activation function. Subsequently, the quantized output Q is obtained by computing the dot product of weight matrix \mathcal{W} and codebook matrix \mathcal{M} , a process that can be conceptualized as a selection operation as shown in Figure 3. To encourage sparsity within the generated weight matrix, we apply a Mean Absolute Error (MAE) loss to the output as a surrogate form of regularization.

Despite the potential feasibility of placing the quantization module either before or after the Translator, we note that post-Translator placement induces significant training insta-

bility in classic VQ, attributable to the non-differentiable nature of the straight-through estimator. Conversely, our SVQ module demonstrates consistent stability during training. For consistency, the quantization module is placed before the Translator in our primary experiments, with a comparative assessment of its alternative placement provided in Section B.1.

4. Efficient Utilize of Cookbook Using Sparse Regression

To understand the difference between sparse regression-based quantization scheme and clustering-based quantization scheme, we measure the number of codes that we need in order to approximate any vector within a unit ball \mathcal{B} with error less than δ . We denote this number by $T(\mathcal{B}, \delta)$. As indicated by the theorem below, using sparse regression, $T(\mathcal{B}, \delta)$ can be reduced from $O(1/\delta^d)$ to $O(1/\delta^p)$, with $p \ll d$ for high dimensional vectors.

Theorem 4.1. $T(\mathcal{B}, \delta)$ for the clustering-based method is at least $1/\delta^d$, while $T(\mathcal{B}, \delta)$ for sparse regression can be $(4d/\delta)^p$, with

$$p \geq \max \left(3, \frac{\log(4/\delta)}{\log \log(2d/\varepsilon)} \right),$$

as long as the non-zero elements used by sparse regression is at least $\frac{4d}{\delta(\log C + p \log(4d) - (p+1) \log \delta)}$.

Proof. To bound $T(\mathcal{B}, \delta)$ for the clustering method, we use the covering number for a unit ball \mathcal{B} , requiring at least $1/\delta^d$ code vectors to approximate any vector within error δ . Considering Ug , with $U = (u_1, \dots, u_m)$, $u_k \sim \mathcal{N}(0, I_d/m)$,

and $g \in \Delta_s$ an s -sparse unit vector, we have:

$$\Pr(\|UU^\top - I\|_2 \geq \gamma) \leq 2d \exp\left(-\frac{m\gamma^2}{3d}\right),$$

implying

$$\|UU^\top - I\|_2 \leq \Delta := \sqrt{\frac{d}{m} \log \frac{2d}{\varepsilon}}$$

with probability at least $1 - \varepsilon$. Thus, $\|g' - g\|_2 \geq (1 + \Delta)^{-1} \|Ug - Ug'\|_2$. With the s -sparse unit vector covering number bounded by $(Cm/s\delta)^s$, we obtain:

$$\left(\frac{Cm}{s\delta}\right)^s \geq \left(1 + \frac{2}{\delta}\right)^d (1 + \Delta)^d,$$

By choosing $m = (4d/\delta)^p$, we have

$$(1 + \Delta)^d \leq \exp(d\Delta) \leq e,$$

yielding $s \log(C'm/\delta) \geq 2d/\delta + s \log s$, given $C' = Ce$.

As $s \geq 4d/[\delta(\log C + p \log(4d) - (p+1) \log \delta)]$, it is easy to verify that $s \log s \leq 2d/\delta$, leading to $m \geq (4d/\delta)^p$.

5. Experiments

We extensively evaluate SVQ on a wide range of real-world spatio-temporal forecasting datasets under the unified framework of OpenSTL (Tan et al., 2023b). Note that since SimVP holds leading performance across almost all benchmarks, it is adopted as our primary baseline. We begin by comparing the SimVP+SVQ model with state-of-the-art (SOTA) counterparts. Subsequently, we assess the capability of SVQ to enhance various backbones. Finally, we investigate the delicate balance between detail preservation and noise reduction, and conduct experiments with artificial noise injection to show the effect of SVQ on mitigating noise.

Moreover, we provide a comprehensive comparison between SVQ and existing VQ methods in Appendix B.3, evaluating their downstream prediction performance, codebook utilization, and computational efficiency.

Dataset. To evaluate the proposed SVQ, we conduct extensive experiments on five real-world spatio-temporal forecasting tasks, including weather (WeatherBench), traffic flow (TaxiBJ), human pose dynamics (Human3.6M), driving scenes (KittiCaltech), and human actions (KTH Action). More details about datasets are described in Appendix A.1.

Experimental details. In deployment, we found SVQ to be quite robust to codebook size, as its performance remains consistently strong when using a sufficiently large codebook. Therefore, we fix the codebook size at 10,000 for WeatherBench, TaxiBJ, and Human3.6M datasets, and at

6,000 for KittiCaltech and KTH datasets. The hidden dimension of nonlinear projection layer is fixed at 128. Our experiments are conducted on either 1 or 4 NVIDIA V100 32GB GPUs, with a total batch size of 16. More details about backbone architectures, VQ parameters, computational costs, and metrics are described in Appendix A.2, A.3, B.2, and A.5 respectively.

5.1. Benchmarks on various tasks

We explore both fixed (frozen) and learnable versions of SVQ on various forecasting tasks. Interestingly, we find that when codebook size is large, the performance of frozen, randomly-initialized codebook is on par with carefully learned codebook. Our comparison baselines consist of two categories: 1) Non-recurrent models including SimVP (Tan et al., 2022) and TAU (Tan et al., 2023a); 2) Recurrent-based models including ConvLSTM (SHI et al., 2015), PredNet (Lotter et al., 2017), PredRNN (Wang et al., 2017), PredRNN++ (Wang et al., 2018), MIM (Wang et al., 2019b), E3D-LSTM (Wang et al., 2019a), PhyDNet (Guen & Thome, 2020), MAU (Chang et al., 2021), PredRNNv2 (Wang et al., 2022b), and DMVFN (Hu et al., 2023). Baseline results are copied from the original OpenSTL paper (Tan et al., 2023b). To preclude ambiguity, we select the best MetaFormer of SimVP for each dataset, detailed in Appendix A.2.

We present benchmark results of WeatherBench and three video prediction datasets (Human3.6M, KTH, and KittiCaltech) in Tables 1 and 2, respectively. Due to page limit, the benchmark results of TaxiBJ dataset are provided in Appendix B.4. These datasets have different characteristics. WeatherBench and TaxiBJ are macro forecasting tasks with low-frequency collection (30min or 1-6h). Human3.6M features subtle differences between frames as low-frequency signals. KittiCaltech poses challenges due to its rapidly changing backgrounds and limited training data. The KTH dataset, on the other hand, tests the capacity for long-horizon forecasting, requiring the prediction of 20 future frames based on 10 observed frames.

However, despite the distinct characteristics among datasets, a common thread is the need for improved noise reduction coupled with enhanced representational capabilities, which can universally benefit their respective forecasting tasks. Notably, the SimVP+SVQ model achieves either the best or comparable performance across all datasets. For instance, on the WeatherBench-S temperature dataset, SVQ significantly improves the best baseline by **7.9%** ($1.105 \rightarrow 1.018$). On these three popular video prediction tasks, SVQ not only delivers a reduction in forecasting errors (average **9.4%** decrease in MAE), but also significantly improves subjective image quality (average **17.3%** decrease in LPIPS). Additional visualizations of forecasting samples can be found in Appendix D.

Table 1. **WeatherBench results:** Performance comparison for SVQ module and baseline models on WeatherBench. WeatherBench-S is single-variable, one-hour interval forecasting setup trained on data from 2010-2015, validated on 2016, and tested on 2017-2018. WeatherBench-M targets broader application, which is multi-variable, six-hour interval forecasting setup trained on data from 1979-2015, validated on 2016, and tested on 2017-2018. The top two results are highlighted by bold or underlined.

Dataset	Variable	Temperature		Humidity		Wind Component		Total Cloud Cover	
	Model	MSE↓	MAE↓	MSE↓	MAE↓	MSE↓	MAE↓	MSE↓	MAE↓
WeatherBench-S	ConvLSTM(SHI et al., 2015)	1.521	0.7949	35.146	4.012	1.8976	0.9215	0.0494	0.1542
	E3D-LSTM(Wang et al., 2019a)	1.592	0.8059	36.534	4.100	2.4111	1.0342	0.0573	0.1529
	PredRNN(Wang et al., 2017)	1.331	0.7246	37.611	4.096	1.8810	0.9068	0.0550	0.1588
	MIM(Wang et al., 2019b)	1.784	0.8716	36.534	4.100	3.1399	1.1837	0.0573	0.1529
	MAU(Chang et al., 2021)	1.251	0.7036	34.529	4.004	1.9001	0.9194	0.0496	0.1516
	PredRNN++(Wang et al., 2018)	1.634	0.7883	35.146	4.012	1.8727	0.9019	0.0547	0.1543
	PredRNN.V2(Wang et al., 2022b)	1.545	0.7986	36.508	4.087	2.0072	0.9413	0.0505	0.1587
	TAU(Tan et al., 2023a)	1.162	0.6707	31.831	3.818	1.5925	0.8426	0.0472	0.1460
	SimVP (w/o VQ)(Tan et al., 2022)	1.105	0.6567	31.332	3.776	1.4996	0.8145	0.0466	0.1469
	SimVP+SVQ (Frozen)	<u>1.023</u>	<u>0.6131</u>	<u>30.863</u>	<u>3.661</u>	<u>1.4337</u>	<u>0.7861</u>	0.0456	0.1456
	SimVP+SVQ (Learnable)	1.018	0.6109	30.611	3.657	1.4186	0.7858	<u>0.0458</u>	0.1463
Improvement	↑7.9%	↑7.0%	↑2.3%	↑3.2%	↑5.4%	↑3.5%	↑2.1%	↑0.9%	
WeatherBench-M	Variable	Temperature		Humidity		Wind U Component		Wind V Component	
	ConvLSTM(SHI et al., 2015)	6.303	1.7695	368.15	13.490	30.002	3.8923	30.789	3.8238
	PredRNN(Wang et al., 2017)	5.596	1.6411	354.57	13.169	27.484	3.6776	28.973	3.6617
	MIM(Wang et al., 2019b)	7.515	1.9650	408.24	14.658	35.586	4.2842	36.464	4.2066
	MAU(Chang et al., 2021)	5.628	1.6810	363.36	13.503	27.582	3.7409	27.929	3.6700
	PredRNN++(Wang et al., 2018)	5.647	1.6433	363.15	13.246	28.396	3.7322	29.872	3.7067
	PredRNN.V2(Wang et al., 2022b)	6.307	1.7770	368.52	13.594	29.833	3.8870	31.119	3.8406
	TAU(Tan et al., 2023a)	4.904	1.5341	<u>342.63</u>	12.801	24.719	3.5060	25.456	3.4723
	SimVP (w/o VQ)(Tan et al., 2022)	4.833	1.5246	340.06	12.738	24.535	3.4882	25.232	3.4509
	SimVP+SVQ (Frozen)	4.427	1.4160	360.15	12.445	<u>23.915</u>	<u>3.4078</u>	24.968	<u>3.4117</u>
	SimVP+SVQ (Learnable)	<u>4.433</u>	<u>1.4164</u>	360.53	<u>12.449</u>	23.908	3.4060	<u>24.983</u>	3.4095
Improvement	↑8.4%	↑7.1%	↓5.9%	↑2.3%	↑2.6%	↑2.4%	↑1.0%	↑1.2%	

Table 2. **Video prediction results:** Performance comparison for SVQ module and baseline models on Human3.6M, KTH, and KittiCaltech. The top two results are highlighted by bold or underlined.

Dataset	Human3.6M				KittiCaltech				KTH			
	MAE↓	SSIM↑	PSNR↑	LPIPS↓	MAE↓	SSIM↑	PSNR↑	LPIPS↓	MAE↓	SSIM↑	PSNR↑	LPIPS↓
ConvLSTM(SHI et al., 2015)	1583.3	0.9813	33.40	0.03557	1583.3	0.9345	27.46	0.08575	445.5	0.8977	26.99	0.26686
E3D-LSTM(Wang et al., 2019a)	1442.5	0.9803	32.52	0.04133	1946.2	0.9047	25.45	0.12602	892.7	0.8153	21.78	0.48358
PredNet(Lotter et al., 2017)	1625.3	0.9786	31.76	0.03264	1568.9	0.9286	27.21	0.11289	783.1	0.8094	22.45	0.32159
PhyDNet(Guen & Thome, 2020)	1614.7	0.9804	39.84	0.03709	2754.8	0.8615	23.26	0.32194	765.6	0.8322	23.41	0.50155
MAU(Chang et al., 2021)	1577.0	0.9812	33.33	0.03561	1800.4	0.9176	26.14	0.09673	471.2	0.8945	26.73	0.25442
MIM(Wang et al., 2019b)	1467.1	0.9829	33.97	0.03338	1464.0	0.9409	28.10	0.06353	380.8	0.9025	27.78	0.18808
PredRNN(Wang et al., 2017)	1458.3	0.9831	33.94	0.03245	1525.5	0.9374	27.81	0.07395	380.6	0.9097	27.95	0.21892
PredRNN++(Wang et al., 2018)	1452.2	0.9832	34.02	0.03196	1453.2	0.9433	28.02	0.13210	370.4	0.9124	28.13	<u>0.19871</u>
PredRNN.V2(Wang et al., 2022b)	1484.7	0.9827	33.84	0.03334	1610.5	0.9330	27.12	0.08920	368.8	0.9099	28.01	0.21478
TAU(Tan et al., 2023a)	1390.7	<u>0.9839</u>	34.03	0.02783	1507.8	0.9456	27.83	0.05494	421.7	0.9086	27.10	0.22856
DMVFN(Hu et al., 2023)	-	-	-	-	1531.1	0.9314	26.95	0.04942	413.2	0.8976	26.65	0.12842
SimVP (w/o VQ)(Tan et al., 2022)	1441.0	0.9834	<u>34.08</u>	0.03224	1507.7	0.9453	27.89	0.05740	397.1	0.9065	27.46	0.26496
SimVP+SVQ (Frozen)	1264.9	0.9851	34.07	<u>0.02380</u>	1408.6	0.9469	28.10	0.05535	<u>364.6</u>	0.9109	27.28	0.20988
SimVP+SVQ (Learnable)	<u>1265.1</u>	0.9851	34.06	0.02367	<u>1414.9</u>	<u>0.9458</u>	28.10	0.05776	360.2	<u>0.9116</u>	27.37	0.20658
Improvement	↑12.2%	↑0.2%	↓0.0%	↑26.2%	↑6.6%	↑0.2%	↑0.8%	↑3.6%	↑9.3%	↑0.6%	↓0.3%	↑22.0%

5.2. Boosting performance as a versatile plug-in

In this section, SVQ serves as a versatile plug-in module applicable to various MetaFormers (Yu et al., 2022a). The adopted MetaFormers can be categorized into three types. 1) CNN-based: SimVPv1(IncepU) (Gao et al., 2022), SimVPv2(gSTA) (Tan et al., 2022), ConvMixer (Trockman & Kolter, 2023), ConvNeXt (Liu et al., 2022a), HorNet (Rao et al., 2022), and MogaNet (Li et al., 2022). 2) Transformer-based: ViT (Dosovitskiy et al., 2021), Swin Transformer (Liu et al., 2021), Uniformer (Li et al., 2023), Poolformer (Yu et al., 2022b), and VAN (Guo et al., 2023). 3) MLP-based: MLPmixer (Tolstikhin et al., 2021). We conduct experiments on WeatherBench-S temperature dataset because it is lightweight and fast for training.

As shown in Table 3, SVQ consistently improves the perfor-

mance across all MetaFormers, showcasing its universality across diverse backbone types. We observe an average reduction in MSE and MAE by **4.8%** and **6.0%**, respectively. In detail, SVQ leads to an average MSE reduction of 4.1% for CNN-based backbones, 5.1% for transformer-based, and 10.7% for MLP-based. The more pronounced enhancement in transformer-based and MLP-based models indicates that our approach is especially effective with architectures that prioritize global interactions. Notably, SimVPv2(gSTA) is the best backbone, while our SVQ further improves it by 7.9%. These findings also aligns with our motivation that mitigating noise in the learning process significantly benefits spatio-temporal forecasting, irrespective of model architecture. By integrating SVQ to constrain the diversity of predicted patterns and cut out noise, researchers can focus on crafting high-quality and general base models.

Table 3. **Boosting performance:** The effect of SVQ for various MetaFormers on WeatherBench-S temperature dataset.

MetaFormer	MSE		MAE	
	w/o SVQ	w SVQ	w/o SVQ	w SVQ
SimVPv1(IncepU)(Gao et al., 2022)	1.238	1.216	0.7037	0.6831
SimVPv2(gSTA)(Tan et al., 2022)	1.105	1.018	0.6567	0.6109
ConvMixer(Trockman & Kolter, 2023)	1.267	1.257	0.7073	0.6780
ConvNeXt(Liu et al., 2022a)	1.277	1.159	0.7220	0.6568
HorNet(Rao et al., 2022)	1.201	1.130	0.6906	0.6472
MogaNet(Li et al., 2022)	1.152	1.067	0.6665	0.6271
ViT(Dosovitskiy et al., 2021)	1.146	1.111	0.6712	0.6375
Swin(Liu et al., 2021)	1.143	1.088	0.6735	0.6320
Uniformer(Li et al., 2023)	1.204	1.110	0.6885	0.6400
Poolformer(Yu et al., 2022b)	1.156	1.097	0.6715	0.6297
VAN(Guo et al., 2023)	1.150	1.083	0.6803	0.6342
MLP-Mixer(Tolstikhin et al., 2021)	1.255	1.120	0.7011	0.6455
Average improvement		↑ 4.8%		↑ 6.0%

5.3. Delicate balance between detail preservation and noise reduction

Investigating vector quantization’s (VQ) role in spatio-temporal forecasting, we evaluated several cutting-edge VQ methods akin to the SVQ framework, implemented as plug-in modules coordinated with the primary model. Table 4 shows that SVQ markedly improves forecasting as a plug-in, whereas other VQ approaches generally lead to heightened prediction errors. Enhanced detail retention within the representational capacity is linked to lower forecasting errors. Classic VQ methods suffer from notable information losses, as evidenced by a higher MSE of 1.854. In contrast, both residual VQ and grouped residual VQ outperform traditional VQ with lower MSEs of 1.213 and 1.174, respectively, affirming their ability to preserve intricate details.

It is commonly understood that the size of the codebook in clustering-based VQ is critical: larger codebooks capture more details, whereas smaller ones enhance noise reduction. To explore this trade-off, we analyzed how the codebook size influences the prediction MSE in grouped residual VQ. As Figure 4 indicates, MSE initially decreases but increases with overly large codebooks, echoing findings from (Yu et al., 2023b) that an excessively large codebook may degrade image generation performance. This underscores the necessity for dataset-specific tuning in clustering-based VQ approaches. In contrast, SVQ naturally balances detail preservation and noise reduction using sparse regression, negating the need for such fine-tuning. The codebook size in our approach exhibits a low-maintenance profile: performance remains solid across various codebook sizes, suggesting that utilizing a default large codebook can yield robust results without the need for extensive tuning. We are not suggesting that our SVQ outperforms other VQ methods in general image generation tasks, as this is beyond the scope of our current objective. Rather, we emphasize SVQ’s effectiveness as a noise reduction tool that directly enhances real-world spatio-temporal forecasting tasks, while the application to general image generation remains a topic for

future exploration.

Table 4. **Comparison of vector quantization methods:** All methods share identical backbone, with the recommended setting as described in Appendix A.3. The performance enhancements over baseline are highlighted in bold.

Method	MSE↓	MAE↓
Baseline (SimVP w/o VQ)	1.105	0.6567
VQ(van den Oord et al., 2017)	1.854	0.8963
Residual VQ(Zeghidour et al., 2022)	1.213	0.6910
Grouped Residual VQ(Yang et al., 2023)	1.174	0.6747
Multi-headed VQ(Mama et al., 2021b)	1.211	0.6994
Residual VQ (Stochastic)(Lee et al., 2022)	1.888	0.9237
Residual Finite Scalar Quantization(Mama et al., 2021a)	1.319	0.7505
Lookup Free Quantization (LFQ)(Yu et al., 2023a)	2.988	1.1103
Residual LFQ(Yu et al., 2023a)	1.281	0.7281
SVQ-raw(Xiao et al., 2023)	1.123	0.6456
SVQ	1.018	0.6109

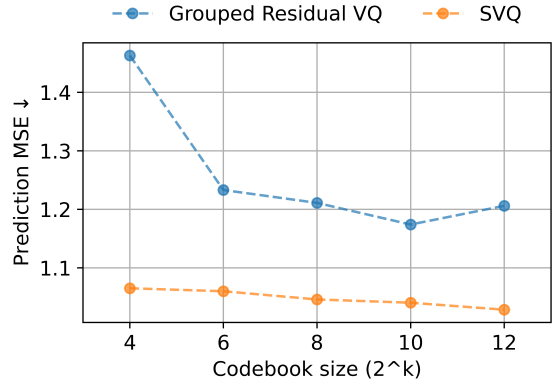


Figure 4. **Prediction MSE curves** on WeatherBench-S temperature dataset with Grouped Residual VQ and SVQ.

5.4. Robustness to artificial noise injection

To clearly demonstrate the noise reduction effect of SVQ, we conduct an experiment by adding artificial noise to the training data. Table 5 shows that the SVQ-equipped model experiences a much lower rise in MSE and MAE relative to the model without SVQ, regardless of the proportion of injected noise. For instance, when the proportion of injected noise is 10%, the MSE of the model without SVQ rises by 25.4%, whereas the model with SVQ shows a modest increase of just 3.2%. These results explicitly confirm that our method effectively mitigates noise by constraining latent patterns via quantization.

Table 5. **Noise injection analysis:** The proportion of injected noise is indicated by η . We present MSE and MAE, and their percentage increase over baseline without artificial noise.

Noise proportion	MSE		MAE	
	w/o SVQ	w SVQ	w/o SVQ	w SVQ
$\eta=0$	1.105	1.018	0.6567	0.6109
$\eta=10\%$	1.386(+25.4%)	1.051(+3.2%)	0.7702(+17.3%)	0.6269(+2.6%)
$\eta=20\%$	1.554(+40.7%)	1.196(+17.5%)	0.8282(+26.1%)	0.6710(+9.8%)
$\eta=30\%$	1.750(+58.4%)	1.255(+23.2%)	0.8821(+34.3%)	0.6953(+13.8%)
$\eta=40\%$	2.081(+88.3%)	1.568(+54.0%)	1.0031(+52.7%)	0.7973(+30.5%)
$\eta=50\%$	2.646(+139.4%)	1.529(+50.2%)	1.1339(+72.7%)	0.7881(+29.0%)

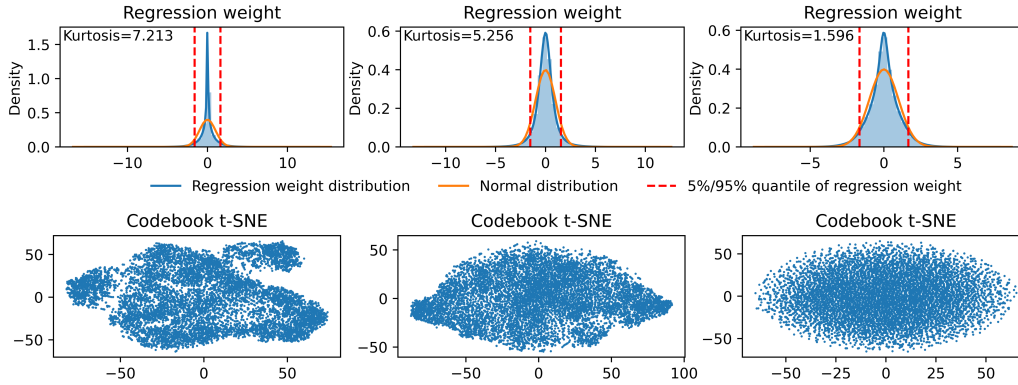


Figure 5. Distribution of regression weight \mathcal{W} and codebook \mathcal{M} : Higher kurtosis represents more compact and concentrate distribution near zero, as well as sparser regression weights. Left: Learnable SVQ with MAE loss. Middle: Learnable SVQ with MSE loss. Right: Frozen SVQ with MAE loss. Learnable setting and MAE loss encourage sparser weights and a more structured codebook.

5.5. Ablation study

We conduct a series of ablation studies on WeatherBench-S temperature dataset to understand the contribution of important designs based on the default setting: SVQ with 10000 codebook size, learnable codebook, and MAE loss.

Codebook size and learnability. We compare the effect of codebook size when codebook is learnable or frozen (Table 6). The results indicate that that increasing codebook size gradually improves performance. When significantly increasing codebook size to a large value, such as 10000, the performance difference between frozen and learnable codebook narrows, evidenced by a mere 0.5% (1.023 \rightarrow 1.018). We observe that enlarging the codebook ensures comprehensive latent space coverage through random codes, negating the need for meticulous learning and allowing random initializations to rival learned counterparts. Additionally, our tailored SVQ structure surpasses alternative designs, including single-layer, bucket-shaped, and post-ReLU variants, while maintaining a similar parameter count.

Table 6. Ablation of model structure.

Learnability	Projection dim	Codebook size	MSE \downarrow	MAE \downarrow
Frozen	128	10	1.070	0.6227
	128	1000	1.044	0.6198
	128	10000	1.023	0.6131
Learnable	128	10	1.060	0.6194
	128	1000	1.048	0.6182
	128	10000	1.018	0.6109
	1280(Bucket-shape)	1280	1.035	0.6149
	None(One-layer)	10000	1.043	0.6144
	128(Post-ReLU)	10000	1.032	0.6136

Self-learned sparse regression structure. The original SimVP model adopts MSE as prediction loss. We individually replace it with MAE loss and add the SVQ module. The results show that the joint use of SVQ and MAE loss is crucial for significantly improving the model’s performance (Table 7). We suggest that the sparsity of the weight matrix \mathcal{W} impacts vector representation learning and use kurtosis to quantify this after normalizing \mathcal{W} . Figure 5 demonstrates that both a learnable codebook and MAE loss contribute to

increased sparsity. Analyzing four codebook initialization methods, in both learnable and fixed settings (Table 8), we find that a learnable codebook promotes sparsity irrespective of the initialization, indicating that sparsity is a self-learned property that enhances intermediate representation learning.

Table 7. Module ablation.

Module	MSE \downarrow	MAE \downarrow
SimVP (MSE loss)	1.105	0.6567
SimVP (MAE loss)	1.126	0.6509
SimVP+SVQ (Learnable, MSE loss)	1.099	0.6527
SimVP+SVQ (Learnable, MAE loss)	1.018	0.6109

Table 8. Ablation of codebook initialization method.

Initialization	Learnability	MSE \downarrow	MAE \downarrow	Kurtosis
kaiming uniform	Frozen	1.023	0.6131	1.596
	Learnable	1.018	0.6109	7.213
sparse(sparsity=0.9)	Frozen	1.050	0.6183	4.165
	Learnable	1.034	0.6160	41.558
trunc normal	Frozen	1.049	0.6166	1.582
	Learnable	1.031	0.6161	4.236
orthogonal	Frozen	1.034	0.6170	1.561
	Learnable	1.030	0.6131	35.774

6. Conclusions

In this work, we present Sparse regression-based Vector Quantization (SVQ), a concise yet effective method for spatiotemporal forecasting enhancement. SVQ elegantly balances detail preservation and noise reduction using sparse regression, realized via a two-layer MLP and a codebook, offering computational efficiency and full differentiability. Tested across diverse benchmarks, from weather to traffic and video prediction, SVQ consistently outperforms existing models, setting new performance standards without complex priors. Its differentiability and seamless integration with baseline models highlight SVQ as a significant advancement for efficient and effective spatio-temporal forecasting.

Impact Statements

This paper presents work whose goal is to advance the field of Machine Learning. There are many potential societal consequences of our work, none which we feel must be specifically highlighted here.

References

- Chang, H., Zhang, H., Jiang, L., Liu, C., and Freeman, W. T. Maskgit: Masked generative image transformer. In *IEEE/CVF Conference on Computer Vision and Pattern Recognition, CVPR 2022, New Orleans, LA, USA, June 18-24, 2022*, pp. 11305–11315. IEEE, 2022. doi: 10.1109/CVPR52688.2022.01103. URL <https://doi.org/10.1109/CVPR52688.2022.01103>.
- Chang, Z., Zhang, X., Wang, S., Ma, S., Ye, Y., Xinguang, X., and Gao, W. MAU: A motion-aware unit for video prediction and beyond. In Ranzato, M., Beygelzimer, A., Dauphin, Y. N., Liang, P., and Vaughan, J. W. (eds.), *Advances in Neural Information Processing Systems 34: Annual Conference on Neural Information Processing Systems 2021, NeurIPS 2021, December 6-14, 2021, virtual*, pp. 26950–26962, 2021. URL <https://proceedings.neurips.cc/paper/2021/hash/e25cfa90f04351958216f97e3efdbae9-Abstract.html>.
- Chiu, C.-C., Qin, J., Zhang, Y., Yu, J., and Wu, Y. Self-supervised learning with random-projection quantizer for speech recognition. In *International Conference on Machine Learning*, 2022.
- Dollár, P., Wojek, C., Schiele, B., and Perona, P. Pedestrian detection: A benchmark. In *2009 IEEE Computer Society Conference on Computer Vision and Pattern Recognition (CVPR 2009), 20-25 June 2009, Miami, Florida, USA*, pp. 304–311. IEEE Computer Society, 2009. doi: 10.1109/CVPR.2009.5206631. URL <https://doi.org/10.1109/CVPR.2009.5206631>.
- Dosovitskiy, A., Beyer, L., Kolesnikov, A., Weissenborn, D., Zhai, X., Unterthiner, T., Dehghani, M., Minderer, M., Heigold, G., Gelly, S., Uszkoreit, J., and Houshy, N. An image is worth 16x16 words: Transformers for image recognition at scale. In *9th International Conference on Learning Representations, ICLR 2021, Virtual Event, Austria, May 3-7, 2021*. OpenReview.net, 2021. URL <https://openreview.net/forum?id=YicbFdNTTy>.
- Esser, P., Rombach, R., and Ommer, B. Taming transformers for high-resolution image synthesis. In *IEEE Conference on Computer Vision and Pattern Recognition, CVPR 2021, virtual, June 19-25, 2021*, pp. 12873–12883. Computer Vision Foundation / IEEE, 2021. doi: 10.1109/CVPR46437.2021.01268. URL https://openaccess.thecvf.com/content/CVPR2021/html/Esser_Taming_Transformers_for_High-Resolution_Image_Synthesis_CVPR_2021_paper.html.
- Gao, Z., Tan, C., Wu, L., and Li, S. Z. Simvp: Simpler yet better video prediction. In *IEEE/CVF Conference on Computer Vision and Pattern Recognition, CVPR 2022, New Orleans, LA, USA, June 18-24, 2022*, pp. 3160–3170. IEEE, 2022. doi: 10.1109/CVPR52688.2022.00317. URL <https://doi.org/10.1109/CVPR52688.2022.00317>.
- Geiger, A., Lenz, P., Stiller, C., and Urtasun, R. Vision meets robotics: The KITTI dataset. *Int. J. Robotics Res.*, 32(11):1231–1237, 2013. doi: 10.1177/0278364913491297. URL <https://doi.org/10.1177/0278364913491297>.
- Gregor, K. and LeCun, Y. Learning fast approximations of sparse coding. In Fürnkranz, J. and Joachims, T. (eds.), *Proceedings of the 27th International Conference on Machine Learning (ICML-10), June 21-24, 2010, Haifa, Israel*, pp. 399–406. Omnipress, 2010. URL <https://icml.cc/Conferences/2010/papers/449.pdf>.
- Guen, V. L. and Thome, N. Disentangling physical dynamics from unknown factors for unsupervised video prediction. In *2020 IEEE/CVF Conference on Computer Vision and Pattern Recognition, CVPR 2020, Seattle, WA, USA, June 13-19, 2020*, pp. 11471–11481. Computer Vision Foundation / IEEE, 2020. doi: 10.1109/CVPR42600.2020.01149. URL https://openaccess.thecvf.com/content_CVPR_2020/html/Le_Guen_Disentangling_Physical_Dynamics_From_Unknown_Factors_for_Unsupervised_Video_Prediction_CVPR_2020_paper.html.
- Guo, M., Lu, C., Liu, Z., Cheng, M., and Hu, S. Visual attention network. *Comput. Vis. Media*, 9(4):733–752, 2023. doi: 10.1007/S41095-023-0364-2. URL <https://doi.org/10.1007/s41095-023-0364-2>.
- Hu, X., Huang, Z., Huang, A., Xu, J., and Zhou, S. A dynamic multi-scale voxel flow network for video prediction. In *IEEE/CVF Conference on Computer Vision and Pattern Recognition, CVPR 2023, Vancouver, BC, Canada, June 17-24, 2023*, pp. 6121–6131. IEEE, 2023. doi: 10.1109/CVPR52729.2023.00593. URL <https://doi.org/10.1109/CVPR52729.2023.00593>.

- Ionescu, C., Papava, D., Olaru, V., and Sminchisescu, C. Human3.6m: Large scale datasets and predictive methods for 3d human sensing in natural environments. *IEEE Trans. Pattern Anal. Mach. Intell.*, 36(7):1325–1339, 2014. doi: 10.1109/TPAMI.2013.248. URL <https://doi.org/10.1109/TPAMI.2013.248>.
- Lee, D., Kim, C., Kim, S., Cho, M., and Han, W. Autoregressive image generation using residual quantization. In *IEEE/CVF Conference on Computer Vision and Pattern Recognition, CVPR 2022, New Orleans, LA, USA, June 18-24, 2022*, pp. 11513–11522. IEEE, 2022. doi: 10.1109/CVPR52688.2022.01123. URL <https://doi.org/10.1109/CVPR52688.2022.01123>.
- Li, K., Wang, Y., Zhang, J., Gao, P., Song, G., Liu, Y., Li, H., and Qiao, Y. Uniformer: Unifying convolution and self-attention for visual recognition. *IEEE Trans. Pattern Anal. Mach. Intell.*, 45(10):12581–12600, 2023. doi: 10.1109/TPAMI.2023.3282631. URL <https://doi.org/10.1109/TPAMI.2023.3282631>.
- Li, S., Wang, Z., Liu, Z., Tan, C., Lin, H., Wu, D., Chen, Z., Zheng, J., and Li, S. Z. Efficient multi-order gated aggregation network. *CoRR*, abs/2211.03295, 2022. doi: 10.48550/ARXIV.2211.03295. URL <https://doi.org/10.48550/arXiv.2211.03295>.
- Liu, Z., Lin, Y., Cao, Y., Hu, H., Wei, Y., Zhang, Z., Lin, S., and Guo, B. Swin transformer: Hierarchical vision transformer using shifted windows. In *2021 IEEE/CVF International Conference on Computer Vision, ICCV 2021, Montreal, QC, Canada, October 10-17, 2021*, pp. 9992–10002. IEEE, 2021. doi: 10.1109/ICCV48922.2021.00986. URL <https://doi.org/10.1109/ICCV48922.2021.00986>.
- Liu, Z., Mao, H., Wu, C., Feichtenhofer, C., Darrell, T., and Xie, S. A convnet for the 2020s. In *IEEE/CVF Conference on Computer Vision and Pattern Recognition, CVPR 2022, New Orleans, LA, USA, June 18-24, 2022*, pp. 11966–11976. IEEE, 2022a. doi: 10.1109/CVPR52688.2022.01167. URL <https://doi.org/10.1109/CVPR52688.2022.01167>.
- Liu, Z., Ning, J., Cao, Y., Wei, Y., Zhang, Z., Lin, S., and Hu, H. Video swin transformer. In *IEEE/CVF Conference on Computer Vision and Pattern Recognition, CVPR 2022, New Orleans, LA, USA, June 18-24, 2022*, pp. 3192–3201. IEEE, 2022b. doi: 10.1109/CVPR52688.2022.00320. URL <https://doi.org/10.1109/CVPR52688.2022.00320>.
- Lotter, W., Kreiman, G., and Cox, D. D. Deep predictive coding networks for video prediction and unsupervised learning. In *5th International Conference on Learning Representations, ICLR 2017, Toulon, France, April 24-26, 2017, Conference Track Proceedings*. OpenReview.net, 2017. URL <https://openreview.net/forum?id=B1ewdt9xe>.
- Mama, R., Tyndel, M. S., Kadhim, H., Clifford, C., and Thurairatnam, R. NWT: towards natural audio-to-video generation with representation learning. *CoRR*, abs/2106.04283, 2021a. URL <https://arxiv.org/abs/2106.04283>.
- Mama, R., Tyndel, M. S., Kadhim, H., Clifford, C., and Thurairatnam, R. NWT: towards natural audio-to-video generation with representation learning. *CoRR*, abs/2106.04283, 2021b. URL <https://arxiv.org/abs/2106.04283>.
- Rao, Y., Zhao, W., Tang, Y., Zhou, J., Lim, S., and Lu, J. Hornet: Efficient high-order spatial interactions with recursive gated convolutions. In *NeurIPS*, 2022. URL http://papers.nips.cc/paper_files/paper/2022/hash/436d042b2dd81214d23ae43eb196b146-Abstract-Conference.html.
- Rasp, S., Dueben, P. D., Scher, S., Weyn, J. A., Moutatid, S., and Thuerey, N. Weatherbench: a benchmark data set for data-driven weather forecasting. *Journal of Advances in Modeling Earth Systems*, 12(11):e2020MS002203, 2020.
- Schüldt, C., Laptev, I., and Caputo, B. Recognizing human actions: A local SVM approach. In *17th International Conference on Pattern Recognition, ICPR 2004, Cambridge, UK, August 23-26, 2004*, pp. 32–36. IEEE Computer Society, 2004. doi: 10.1109/ICPR.2004.1334462. URL <https://doi.org/10.1109/ICPR.2004.1334462>.
- SHI, X., Chen, Z., Wang, H., Yeung, D.-Y., Wong, W.-k., and WOO, W.-c. Convolutional lstm network: A machine learning approach for precipitation nowcasting. In Cortes, C., Lawrence, N., Lee, D., Sugiyama, M., and Garnett, R. (eds.), *Advances in Neural Information Processing Systems*, volume 28. Curran Associates, Inc., 2015. URL <https://proceedings.neurips.cc/paper/2015/file/07563a3fe3bbe7e3ba84431ad9d055af-Paper.pdf>.
- Tan, C., Gao, Z., and Li, S. Z. Simvp: Towards simple yet powerful spatiotemporal predictive learning. *CoRR*, abs/2211.12509, 2022. doi: 10.48550/ARXIV.2211.12509. URL <https://doi.org/10.48550/arXiv.2211.12509>.
- Tan, C., Gao, Z., Wu, L., Xu, Y., Xia, J., Li, S., and Li, S. Z. Temporal attention unit: Towards efficient spatiotemporal

- predictive learning. In *IEEE/CVF Conference on Computer Vision and Pattern Recognition, CVPR 2023, Vancouver, BC, Canada, June 17-24, 2023*, pp. 18770–18782. IEEE, 2023a. doi: 10.1109/CVPR52729.2023.01800. URL <https://doi.org/10.1109/CVPR52729.2023.01800>.
- Tan, C., Li, S., Gao, Z., Guan, W., Wang, Z., Liu, Z., Wu, L., and Li, S. Z. Openstl: A comprehensive benchmark of spatio-temporal predictive learning. *CoRR*, abs/2306.11249, 2023b. doi: 10.48550/ARXIV.2306.11249. URL <https://doi.org/10.48550/arXiv.2306.11249>.
- Tolstikhin, I. O., Houlsby, N., Kolesnikov, A., Beyer, L., Zhai, X., Unterthiner, T., Yung, J., Steiner, A., Keysers, D., Uszkoreit, J., Lucic, M., and Dosovitskiy, A. Mlp-mixer: An all-mlp architecture for vision. In Ranzato, M., Beygelzimer, A., Dauphin, Y. N., Liang, P., and Vaughan, J. W. (eds.), *Advances in Neural Information Processing Systems 34: Annual Conference on Neural Information Processing Systems 2021, NeurIPS 2021, December 6-14, 2021, virtual*, pp. 24261–24272, 2021. URL <https://proceedings.neurips.cc/paper/2021/hash/cba0a4ee5ccd02fda0fe3f9a3e7b89fe-Abstract.html>.
- Trockman, A. and Kolter, J. Z. Patches are all you need? *Trans. Mach. Learn. Res.*, 2023. URL <https://openreview.net/forum?id=rAnB7JSMXL>.
- Tschannen, M., Eastwood, C., and Mentzer, F. Givt: Generative infinite-vocabulary transformers. *ArXiv*, abs/2312.02116, 2023. URL <https://api.semanticscholar.org/CorpusID:265610025>.
- van den Oord, A., Vinyals, O., and Kavukcuoglu, K. Neural discrete representation learning. In Guyon, I., von Luxburg, U., Bengio, S., Wallach, H. M., Fergus, R., Vishwanathan, S. V. N., and Garnett, R. (eds.), *Advances in Neural Information Processing Systems 30: Annual Conference on Neural Information Processing Systems 2017, December 4-9, 2017, Long Beach, CA, USA*, pp. 6306–6315, 2017. URL <https://proceedings.neurips.cc/paper/2017/hash/7a98af17e63a0ac09ce2e96d03992fbc-Abstract.html>.
- Wang, S., Cao, J., and Yu, P. S. Deep learning for spatio-temporal data mining: A survey. *IEEE Transactions on Knowledge and Data Engineering*, 34(8):3681–3700, 2022a. doi: 10.1109/TKDE.2020.3025580.
- Wang, Y., Long, M., Wang, J., Gao, Z., and Yu, P. S. Predrnn: Recurrent neural networks for predictive learning using spatiotemporal lstms. In Guyon, I., von Luxburg, U., Bengio, S., Wallach, H. M., Fergus, R., Vishwanathan, S. V. N., and Garnett, R. (eds.), *Advances in Neural Information Processing Systems 30: Annual Conference on Neural Information Processing Systems 2017, December 4-9, 2017, Long Beach, CA, USA*, pp. 879–888, 2017. URL <https://proceedings.neurips.cc/paper/2017/hash/e5f6ad6ce374177eef023bf5d0c018b6-Abstract.html>.
- Wang, Y., Gao, Z., Long, M., Wang, J., and Yu, P. S. Predrnn+: Towards A resolution of the deep-in-time dilemma in spatiotemporal predictive learning. In Dy, J. G. and Krause, A. (eds.), *Proceedings of the 35th International Conference on Machine Learning, ICML 2018, Stockholmsmässan, Stockholm, Sweden, July 10-15, 2018*, volume 80 of *Proceedings of Machine Learning Research*, pp. 5110–5119. PMLR, 2018. URL <http://proceedings.mlr.press/v80/wang18b.html>.
- Wang, Y., Jiang, L., Yang, M., Li, L., Long, M., and Fei-Fei, L. Eidetic 3d LSTM: A model for video prediction and beyond. In *7th International Conference on Learning Representations, ICLR 2019, New Orleans, LA, USA, May 6-9, 2019*. OpenReview.net, 2019a. URL <https://openreview.net/forum?id=B1lKS2AqtX>.
- Wang, Y., Zhang, J., Zhu, H., Long, M., Wang, J., and Yu, P. S. Memory in memory: A predictive neural network for learning higher-order non-stationarity from spatiotemporal dynamics. In *IEEE Conference on Computer Vision and Pattern Recognition, CVPR 2019, Long Beach, CA, USA, June 16-20, 2019*, pp. 9154–9162. Computer Vision Foundation / IEEE, 2019b. doi: 10.1109/CVPR.2019.00937. URL http://openaccess.thecvf.com/content_CVPR_2019/html/Wang_Memory_in_Memory_A_Predictive_Neural_Network_for_Learning_Higher-Order_CVPR_2019_paper.html.
- Wang, Y., Wu, H., Zhang, J., Gao, Z., Wang, J., Yu, P., and Long, M. Predrnn: A recurrent neural network for spatiotemporal predictive learning. *IEEE Transactions on Pattern Analysis and Machine Intelligence*, pp. 1–1, 2022b. doi: 10.1109/TPAMI.2022.3165153.
- Wang, Z., Bovik, A. C., Sheikh, H. R., and Simoncelli, E. P. Image quality assessment: from error visibility to structural similarity. *IEEE Trans. Image Process.*, 13(4):600–612, 2004. doi: 10.1109/TIP.2003.819861. URL <https://doi.org/10.1109/TIP.2003.819861>.
- Xiao, P., Qiu, P., and Sotiras, A. SC-VAE: sparse coding-based variational autoencoder. *CoRR*, abs/2303.16666,

2023. doi: 10.48550/ARXIV.2303.16666. URL <https://doi.org/10.48550/arXiv.2303.16666>.
- Xu, Z., Wang, Y., Long, M., and Wang, J. Predcnn: Predictive learning with cascade convolutions. In Lang, J. (ed.), *Proceedings of the Twenty-Seventh International Joint Conference on Artificial Intelligence, IJCAI 2018, July 13-19, 2018, Stockholm, Sweden*, pp. 2940–2947. ijcai.org, 2018. doi: 10.24963/IJCAI.2018/408. URL <https://doi.org/10.24963/ijcai.2018/408>.
- Yang, D., Liu, S., Huang, R., Tian, J., Weng, C., and Zou, Y. Hifi-codec: Group-residual vector quantization for high fidelity audio codec. *CoRR*, abs/2305.02765, 2023. doi: 10.48550/ARXIV.2305.02765. URL <https://doi.org/10.48550/arXiv.2305.02765>.
- Yu, L., Lezama, J., Gundavarapu, N. B., Versari, L., Sohn, K., Minnen, D., Cheng, Y., Gupta, A., Gu, X., Hauptmann, A. G., Gong, B., Yang, M., Essa, I., Ross, D. A., and Jiang, L. Language model beats diffusion - tokenizer is key to visual generation. *CoRR*, abs/2310.05737, 2023a. doi: 10.48550/ARXIV.2310.05737. URL <https://doi.org/10.48550/arXiv.2310.05737>.
- Yu, L., Lezama, J., Gundavarapu, N. B., Versari, L., Sohn, K., Minnen, D., Cheng, Y., Gupta, A., Gu, X., Hauptmann, A. G., Gong, B., Yang, M., Essa, I., Ross, D. A., and Jiang, L. Language model beats diffusion - tokenizer is key to visual generation. *CoRR*, abs/2310.05737, 2023b. doi: 10.48550/ARXIV.2310.05737. URL <https://doi.org/10.48550/arXiv.2310.05737>.
- Yu, W., Luo, M., Zhou, P., Si, C., Zhou, Y., Wang, X., Feng, J., and Yan, S. Metaformer is actually what you need for vision. In *IEEE/CVF Conference on Computer Vision and Pattern Recognition, CVPR 2022, New Orleans, LA, USA, June 18-24, 2022*, pp. 10809–10819. IEEE, 2022a. doi: 10.1109/CVPR52688.2022.01055. URL <https://doi.org/10.1109/CVPR52688.2022.01055>.
- Yu, W., Luo, M., Zhou, P., Si, C., Zhou, Y., Wang, X., Feng, J., and Yan, S. Metaformer is actually what you need for vision. In *IEEE/CVF Conference on Computer Vision and Pattern Recognition, CVPR 2022, New Orleans, LA, USA, June 18-24, 2022*, pp. 10809–10819. IEEE, 2022b. doi: 10.1109/CVPR52688.2022.01055. URL <https://doi.org/10.1109/CVPR52688.2022.01055>.
- Zeghidour, N., Luebs, A., Omran, A., Skoglund, J., and Tagliasacchi, M. Soundstream: An end-to-end neural audio codec. *IEEE ACM Trans. Audio Speech Lang. Process.*, 30:495–507, 2022. doi: 10.1109/TASLP.2021.3129994. URL <https://doi.org/10.1109/TASLP.2021.3129994>.
- Zhang, J., Zheng, Y., and Qi, D. Deep spatio-temporal residual networks for citywide crowd flows prediction. In Singh, S. and Markovitch, S. (eds.), *Proceedings of the Thirty-First AAAI Conference on Artificial Intelligence, February 4-9, 2017, San Francisco, California, USA*, pp. 1655–1661. AAAI Press, 2017. doi: 10.1609/AAAI.V31I1.10735. URL <https://doi.org/10.1609/aaai.v31i1.10735>.
- Zhang, R., Isola, P., Efros, A. A., Shechtman, E., and Wang, O. The unreasonable effectiveness of deep features as a perceptual metric. In *2018 IEEE Conference on Computer Vision and Pattern Recognition, CVPR 2018, Salt Lake City, UT, USA, June 18-22, 2018*, pp. 586–595. Computer Vision Foundation / IEEE Computer Society, 2018. doi: 10.1109/CVPR.2018.00068. URL http://openaccess.thecvf.com/content_cvpr_2018/html/Zhang_The_Unreasonable_Effectiveness_CVPR_2018_paper.html.

Supplemental Materials

The supplementary material for our work *A Differentiable Sparse Vector Quantization (SVQ) for Spatio-Temporal Forecasting* is organized as follows: Section A provides implementation details of SimVP model and VQ methods. Section B present extended quantitative results. Section C examines the effect of SVQ on latent representation. Finally, Section D shows additional qualitative results of forecasting samples and errors.

A. Implementation details

A.1. Dataset details

The details of the benchmark datasets are summarized as follows: WeatherBench (Rasp et al., 2020) and TaxiBJ (Zhang et al., 2017) are two macro forecasting tasks. These two datasets are collected at low frequencies (30min or 1-6h) and exhibit stable states, which is especially challenging for the model to capture subtle changes. Human3.6M (Ionescu et al., 2014), KittiCaltech (Geiger et al., 2013; Dollár et al., 2009), and KTH Action (Schüldt et al., 2004) are three popular video prediction tasks. Due to the diversity and complexity of real-world videos, these datasets have totally different characteristics. A summary of dataset statistics is provided in Table 9.

Table 9. The detailed statistics of benchmark datasets.

Dataset	Size		Seq. Len.		Img. Shape H × W × C	Interval
	train	test	in	out		
WeatherBench-S	2,167	706	12	12	32 × 64 × 1	1 hour
WeatherBench-M	54,019	2,883	4	4	32 × 64 × 4	6 hour
TaxiBJ	20,461	500	4	4	32 × 32 × 2	30 min
KittiCaltech	3,160	3,095	10	1	128 × 160 × 3	Frame
Human3.6M	73,404	8,582	4	4	256 × 256 × 3	Frame
KTH Action	4,940	3,030	10	20	128 × 128 × 1	Frame

A.2. Architecture configuration of SimVP

Table 10 reports the architectures of SimVP on all datasets. We select the best MetaFormer to replace the translator module based on OpenSTL benchmarks¹²³. The parameters remain unchanged, following the original configurations. It should be noted that, due to the reproducibility issue of ConvNeXt on the TaxiBJ dataset, we have opted to utilize gSTA as our backbone model.

Table 10. Detailed configuration of SimVP backbone.

Dataset	MetaFormer (Translator)	spatio_kernel	hid_S	hid_T	N_T	N_S	drop_path	LR scheduler
WeatherBench-S temperature	gSTA	enc=3, dec=3	32	256	8	2	0.1	cosine
WeatherBench-S humidity	Swin	enc=3, dec=3	32	256	8	2	0.2	cosine
WeatherBench-S wind component	Swin	enc=3, dec=3	32	256	8	2	0.2	cosine
WeatherBench-S total cloud cover	gSTA	enc=3, dec=3	32	256	8	2	0.1	cosine
WeatherBench-M	MogaNet	enc=3, dec=3	32	256	8	2	0.1	cosine
TaxiBJ	gSTA	enc=3, dec=3	32	256	8	2	0.1	cosine
Human3.6M	gSTA	enc=3, dec=3	64	512	6	4	0.1	cosine
KTH	IncepU	enc=3, dec=3	64	256	6	2	0.1	onecycle
KittiCaltech	gSTA	enc=3, dec=3	64	256	6	2	0.2	onecycle

A.3. Parameters of compared VQ methods

In Table 4, we compared SVQ with a series of well-known VQ methods. These methods are reproduced using the source code provided on the GitHub repository⁴. We maintain the parameters consistent with the recommended settings to guarantee performance, as detailed in Table 11. Importantly, to maintain comparable complexity among the methods, we enable a shared codebook for all quantizers in Residual VQ, as well as across the heads in Multi-headed VQ. Moreover, we also conduct an extensive additional experiment for VQ methods using the same codebook size in Section B.3.

¹https://openstl.readthedocs.io/en/latest/model_zoos/video_benchmarks.html

²https://openstl.readthedocs.io/en/latest/model_zoos/weather_benchmarks.html

³https://openstl.readthedocs.io/en/latest/model_zoos/traffic_benchmarks.html

⁴<https://github.com/lucidrains/vector-quantize-pytorch/tree/master>

Table 11. Parameters of the compared VQ methods.

Vector quantization method	codebook_size	num_quantizers	groups	heads	shared_codebook	Specific parameters
VQ	512	-	-	-	-	-
Residual VQ	1024	8	-	-	✓	-
Grouped Residual VQ	1024	8	2	-	✓	-
Multi-headed VQ	1024	-	-	8	✓	-
Residual VQ (Stochastic)	1024	8	-	-	✓	stochastic_sample_codes=True
Residual Finite Scalar Quantization	-	8	-	-	-	levels=[8, 5, 5, 3]
Lookup Free Quantization (LFQ)	8192	-	-	-	-	entropy_loss_weight=0.1
Residual LFQ	256	8	-	-	-	-

A.4. Evaluation of perplexity

In contrast to other VQ methods that rely on a single code, our SVQ generates multiple regression weights to merge several codes. To evaluate its perplexity, we first normalize the regression weights and then convert them into binary form using a threshold set at θ times the standard deviation, where θ serves as the threshold value. We utilize two thresholds (2 and 3) to obtain reasonable perplexity.

A.5. Metrics

Forecasting accuracy is evaluated using mean squared error (MSE) and mean absolute error (MAE), while the image quality of predicted frames is assessed using structural similarity index measure (SSIM) (Wang et al., 2004), peak signal-to-noise ratio (PSNR), and learned perceptual image patch similarity (LPIPS) (Zhang et al., 2018). The training process is early stopped with a patience of 10, and the models with the minimal loss are saved for subsequent evaluation.

B. Additional quantitative results

B.1. Position of quantization module

To illustrate how the position of quantization module affects representation learning, we consider two designs as shown in Figure 6. In our main experiments, we adopt the first design where quantization is performed before the translator. In this section, we also investigate an alternative design where quantization is performed after the translator. Interestingly, we found that the classic VQ method (van den Oord et al., 2017) suffers pronounced instability and codebook collapse issues under the latter design, as shown in Figure 7. It is essential to highlight that the backbones without VQ maintain their MSE within the acceptable range of approximately 1 to 2 (refer to Table 3). Yet, integrating classic VQ causes a substantial rise in MSE values, exceeding 10 for different backbones—a level considered excessively high. We hypothesize that this instability is attributed to the non-differentiability of the straight-through estimator, which introduces errors into the gradient flow for preceding modules. In contrast, our SVQ module never encounters such issues and remains highly stable throughout training. To maintain the integrity of all VQ methods, we opt for the first design in our principal manuscript, wherein quantization is executed preceding the translator module.

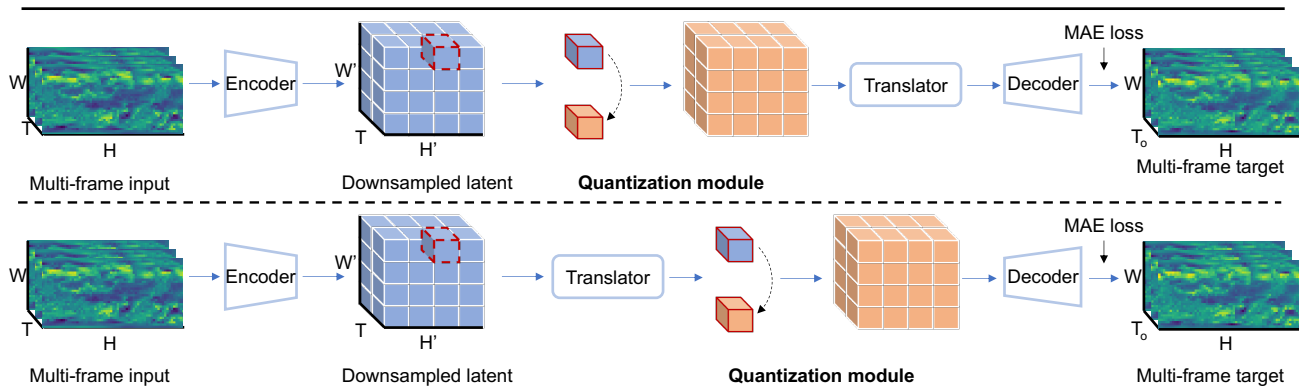


Figure 6. Comparison of two quantization designs with different positions. Top: Quantization before translator. Bottom: Quantization after translator.

A Differentiable Sparse Vector Quantization (SVQ) for Spatio-Temporal Forecasting

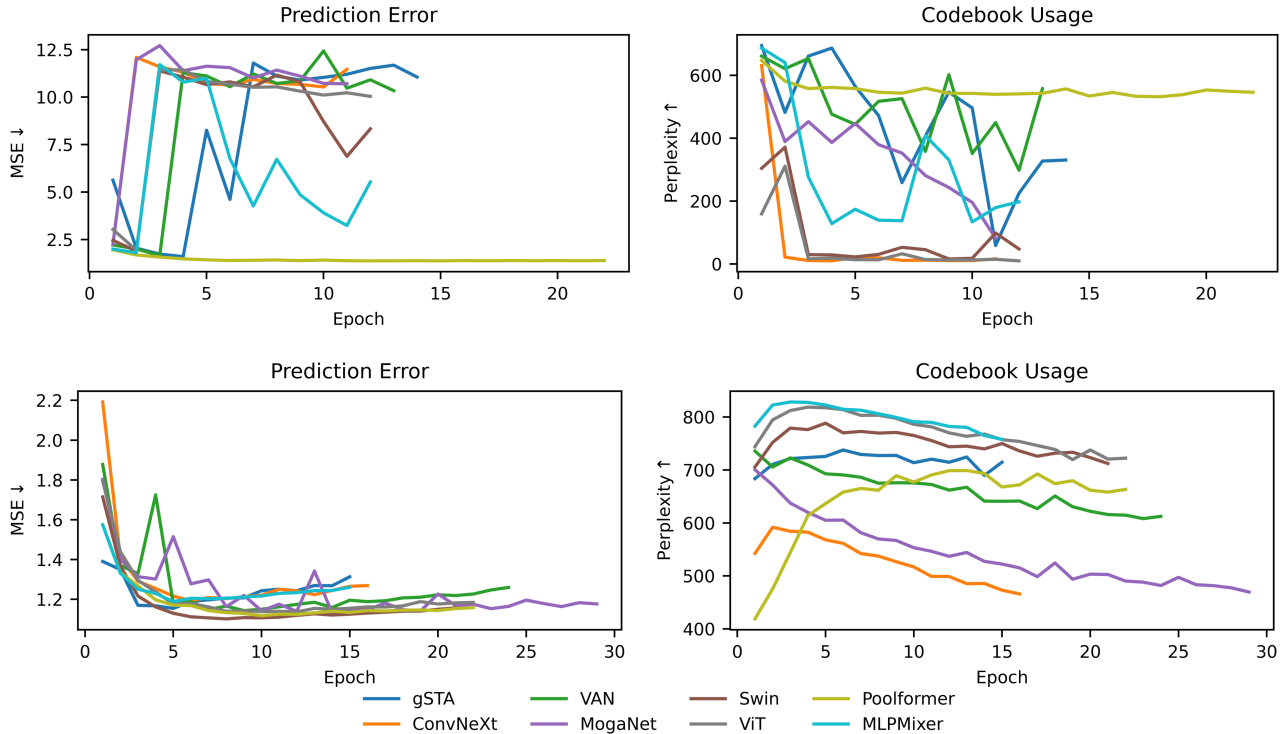


Figure 7. VQ (Top) and SVQ (Bottom) training curves. We perform post-quantization on various backbones, with the same codebook size (1024), employing early stopping (patience of 10) on the WeatherBench-S temperature dataset. Perplexity for SVQ is averaged over different θ values, detailed in Appendix A.4.

B.2. Computational cost

Table 12 presents the computational costs of SVQ module and forecasting models. It shows that recurrent-based models have significantly higher FLOPS requirements, while non-recurrent models are more efficient. The proposed SVQ module is not only effective but also computationally cheap. Across all datasets, SVQ only slightly adds the number of parameters and FLOPS. The computational burden of SimVP+SVQ remains significantly smaller than recurrent-based models.

Table 12. Number of parameters and computing performances for all forecasting models.

Model type	Dataset	Human3.6M		KTH		KittiCaltech		WeatherBench-S		TaxiBJ	
	Model	Params	FLOPS	Params	FLOPS	Params	FLOPS	Params	FLOPS	Params	FLOPS
Recurrent-based	ConvLSTM	15.5M	347.0G	14.9M	1368.0G	15.0M	595.0G	14.98M	136G	14.98M	20.74G
	E3D-LSTM	60.9M	542.0G	53.5M	217.0G	54.9M	1004G	51.09M	169G	50.99M	98.19G
	PredNet	12.5M	13.7G	12.5M	3.4G	12.5M	12.5M	-	-	12.5M	0.85G
	PhyDNet	4.2M	19.1G	3.1M	93.6G	3.1M	40.4G	3.09M	36.8G	3.09M	5.60G
	MAU	20.2M	105.0G	20.1M	399.0G	24.3M	172.0G	5.46M	39.6G	4.41M	6.02G
	MIM	47.6M	1051.0G	39.8M	1099.0G	49.2M	1858G	37.75M	109G	37.86M	64.10G
	PredRNN	24.6M	704.0G	23.6M	2800.0G	23.7M	1216G	23.57M	278G	23.66M	42.40G
	PredRNN++	39.3M	1033.0G	38.3M	4162.0G	38.5M	1803G	38.31M	413G	38.40M	62.95G
	PredRNN.V2	24.6M	708.0G	23.6M	2815.0G	23.8M	1223G	23.59M	279G	23.67M	42.63G
DMVFN	-	-	3.5M	0.88G	3.6M	1.2G	-	-	3.54M	0.057G	
Non-recurrent	TAU	37.6M	182.0G	15.0M	73.8G	44.7M	80.0G	12.22M	6.70G	9.55M	2.49G
	SimVP (w/o VQ)	28.8M	146.0G	12.2M	62.8G	15.6M	96.3G	12.76M	7.01G	7.84M	2.08G
	SimVP+SVQ	30.7M	178.0G	13.3M	110.0G	16.8M	156G	14.37M	16.8G	9.45M	3.72G

B.3. Comprehensive comparison of VQ methods using the same codebook size

To make a fair comparison, we extend Table 4 by setting the codebook size to the same value (1024) for compared VQ methods. They are comprehensively evaluated from different aspects including downstream performance (prediction MSE), codebook usage (perplexity), and computational complexity (FLOPS, inference FPS, and training time per epoch). The

A Differentiable Sparse Vector Quantization (SVQ) for Spatio-Temporal Forecasting

quantitative results are shown in Table 13. The convergence performance is shown in Figure 8, where SVQ quickly converges to the lowest prediction error and satisfactory utilization of the codebook. Residual VQ with stochastic sampling has the highest codebook usage. However, its prediction MSE is worse than residual VQ without stochastic sampling. This demonstrates that codebook usage does not guarantee better downstream performance. SVQ generally outperforms the other VQ methods in computational efficiency, due to the simplified approximation described in Section 3.1.

Table 13. Quantitative comparison of VQ methods with the same codebook size (1024) on WeatherBench-S temperature dataset.

Vector quantization method	Prediction MSE↓	Perplexity↑	FLOPS↓	Inference FPS↑	Training time per epoch(min)↓
VQ	1.8544	51.95	7.207G	21.1	7.11
Residual VQ	1.2131	142.47	8.616G	7.7	13.25
Residual VQ (Stochastic)	1.8882	817.91	8.616G	8.1	17.27
Grouped Residual VQ	1.1737	132.57	8.616G	4.8	19.98
Multi-headed VQ	1.2113	16.36	8.717G	6.2	13.15
SVQ (freeze)	1.0393	335.72($\theta=3$)/438.39($\theta=2$)	8.037G	24.6	7.27
SVQ (Learnable)	1.0403	246.44($\theta=3$)/331.41($\theta=2$)	8.037G	24.9	7.30

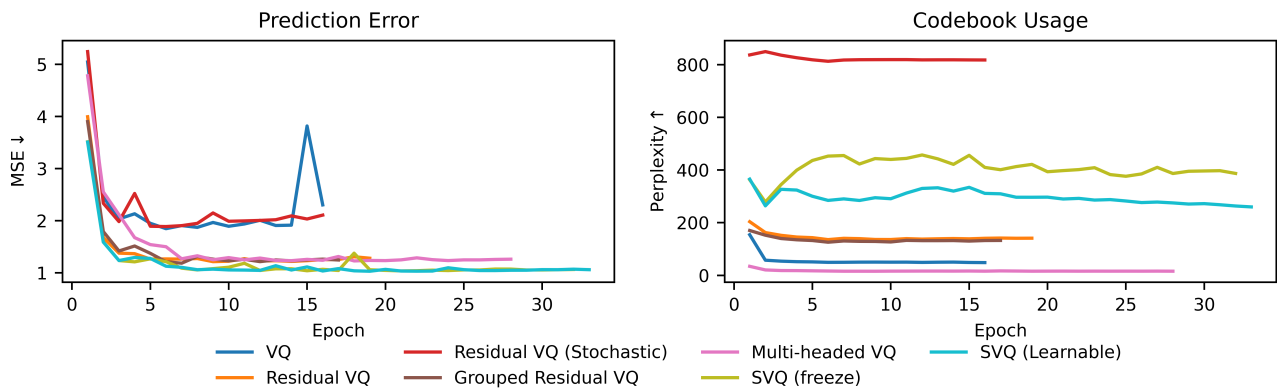


Figure 8. Prediction error and codebook usage of different VQ methods during the training process. All methods adopt the same codebook size (1024) and are early stopped with a patience of 10 on WeatherBench-S temperature dataset. For simplicity, the perplexity of SVQ is averaged on different θ .

B.4. Benchmark on TaxiBJ dataset

Table 14. Performance comparison for SVQ and baseline models on TaxiBJ.

Model	MSE↓	MAE↓	SSIM↑	PSNR↑
ConvLSTM(SHI et al., 2015)	0.3358	15.32	0.9836	39.45
E3D-LSTM(Wang et al., 2019a)	0.3427	14.98	0.9842	39.64
PhyDNet(Guen & Thome, 2020)	0.3622	15.53	0.9828	39.46
PredNet(Lotter et al., 2017)	0.3516	15.91	0.9828	39.29
PredRNN(Wang et al., 2017)	0.3194	15.31	0.9838	39.51
MIM(Wang et al., 2019b)	0.3110	14.96	0.9847	39.65
MAU(Chang et al., 2021)	0.3268	15.26	0.9834	39.52
DMVFN(Hu et al., 2023)	3.3954	45.52	0.8321	31.14
PredRNN++(Wang et al., 2018)	0.3348	15.37	0.9834	39.47
PredRNN.V2(Wang et al., 2022b)	0.3834	15.55	0.9826	39.49
TAU(Tan et al., 2023a)	0.3108	14.93	0.9848	39.74
SimVP (w/o VQ)(Tan et al., 2022)	0.3246	15.03	0.9844	39.71
SimVP+SVQ (Frozen)	0.3171	14.68	0.9848	39.83
SimVP+SVQ (Learnable)	0.3191	14.64	0.9849	39.86
Improvement	↑1.7%	↑2.6%	↑0.1%	↑0.4%

B.5. Ablation of frozen module

The SVQ module consists of a two-layer MLP and a large codebook. The MLP can be seen as a projection from the input vector to the regression weights. In Section 5.5, we have already examined the impact of freezing the codebook on forecasting performance. To further investigate the effect of freezing the two-layer MLP, we conducted an ablation study in

this section. The results, presented in Table 15, show that freezing the codebook only has a slight impact on forecasting performance, while freezing the MLP significantly impairs the performance.

Table 15. Ablation of frozen modules on WeatherBench-S temperature dataset.

Frozen module	None (All learnable)	Codebook	Two-layer MLP projection	Both
MSE	1.018	1.023	1.060	1.093
MAE	0.6109	0.6131	0.6194	0.6387

C. Effect of SVQ on latent representation

We investigated the impact of SVQ on the sparsity of regression weights in Figure 5. To further investigate its effect on the latent representation, we compare the distribution of batch tensors before and after applying SVQ. We transform the tensors into normalized vectors and estimate their density distributions. As depicted in Figure 9, the representation after SVQ demonstrates a more compact distribution, indicating improved robustness to noise. The results further prove that SVQ can enhance forecasting performance by effectively handling noise in the data.

Figures 10, 11, 13, 14, and 12 present the comparison of latent feature maps before and after applying SVQ. These figures illustrate that the difference between foreground and background in the feature maps increases after SVQ. For example, in the KittiCaltech dataset, a clear distinction is observed between road conditions and sky (Figure 10). Similarly, in the WeatherBench-S temperature dataset, distinctive regions are identified between high and low latitudes (Figure 11). These findings suggest that SVQ helps in enhancing the discriminative power of the latent representations, which in turn contributes to improved downstream forecasting performance.

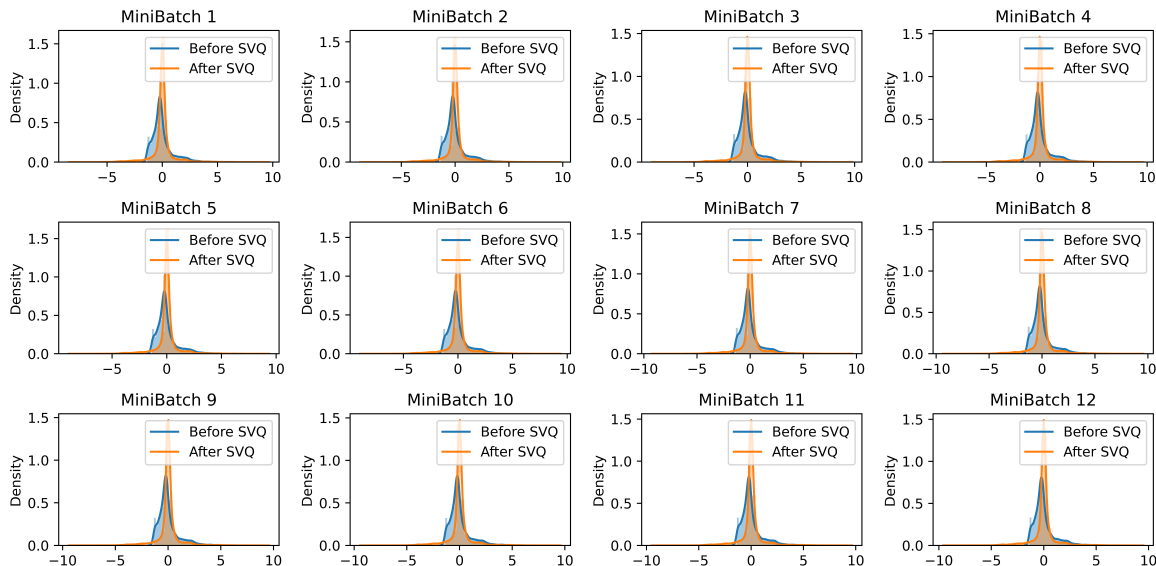


Figure 9. Distribution of latent vector on WeatherBench-S temperature dataset.

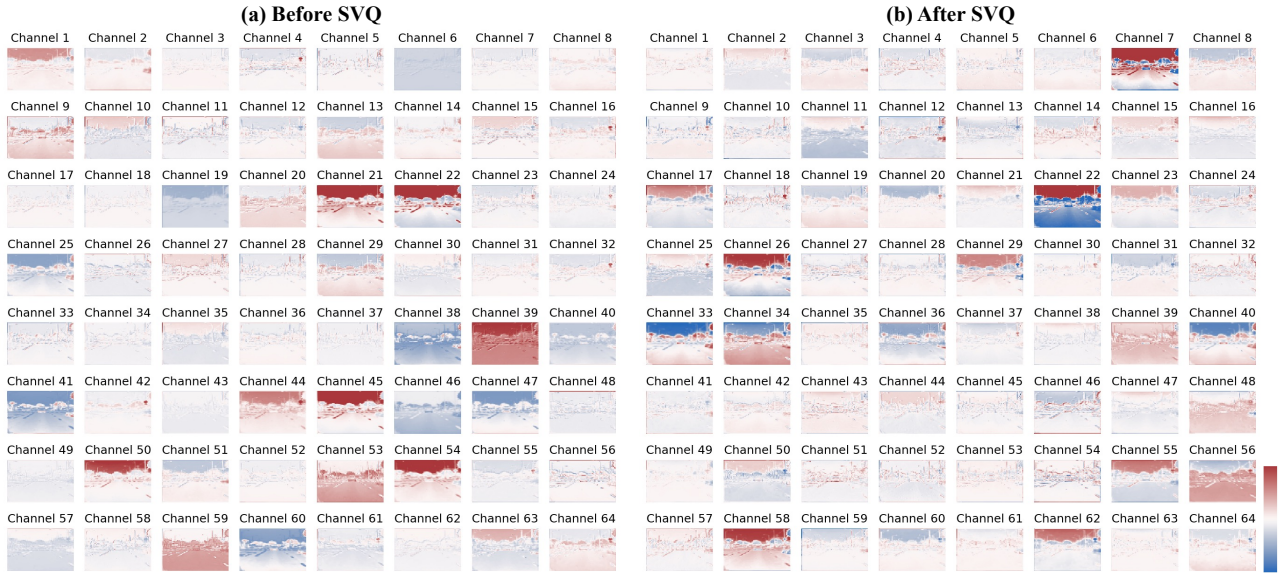


Figure 10. Latent feature map on the KittiCaltech dataset: (a) feature map before SVQ, and (b) feature map after SVQ.

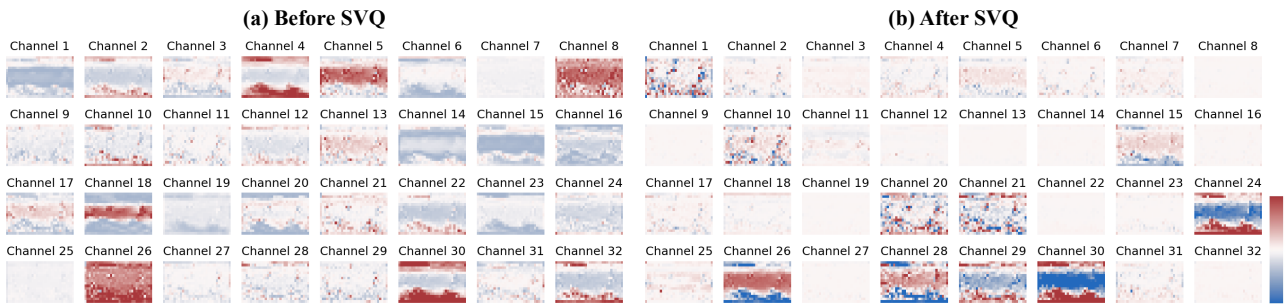


Figure 11. Latent feature map on the WeatherBench-S temperature dataset: (a) feature map before SVQ, and (b) feature map after SVQ.

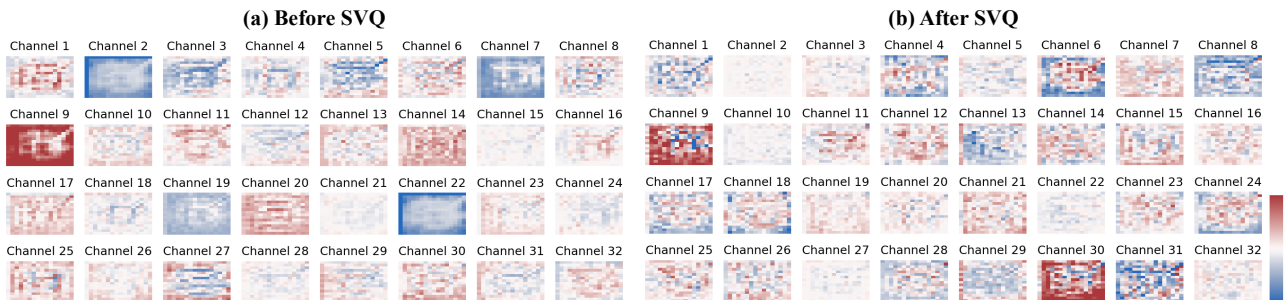


Figure 12. Latent feature map on the TaxiBJ dataset: (a) feature map before SVQ, and (b) feature map after SVQ.

A Differentiable Sparse Vector Quantization (SVQ) for Spatio-Temporal Forecasting

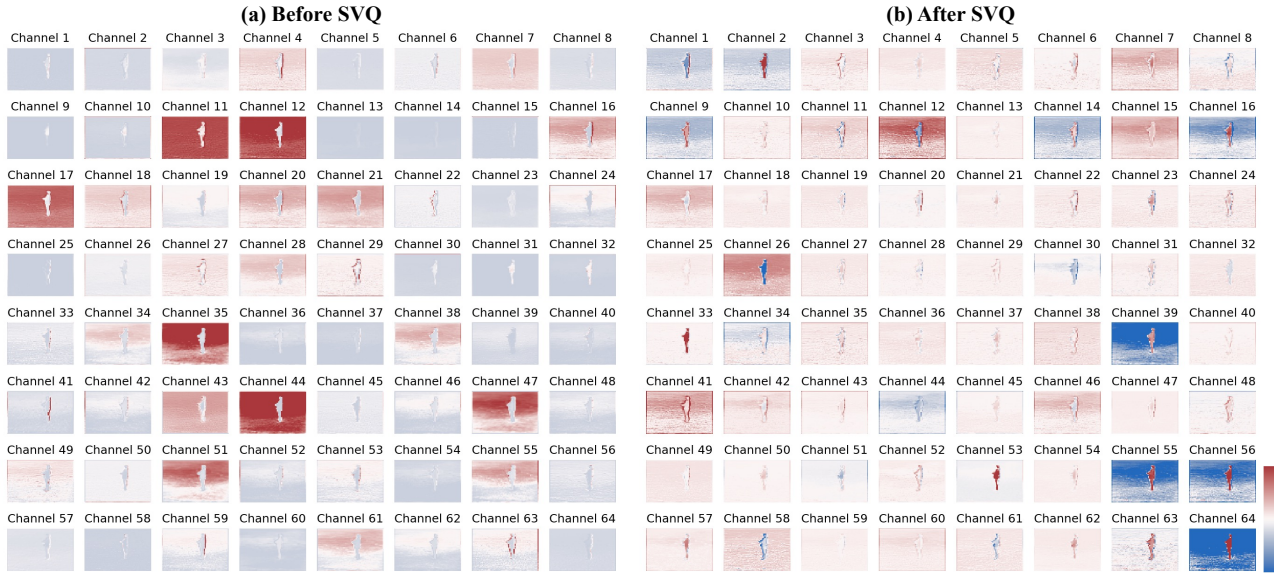


Figure 13. Latent feature map on the KTH dataset: (a) feature map before SVQ, and (b) feature map after SVQ.

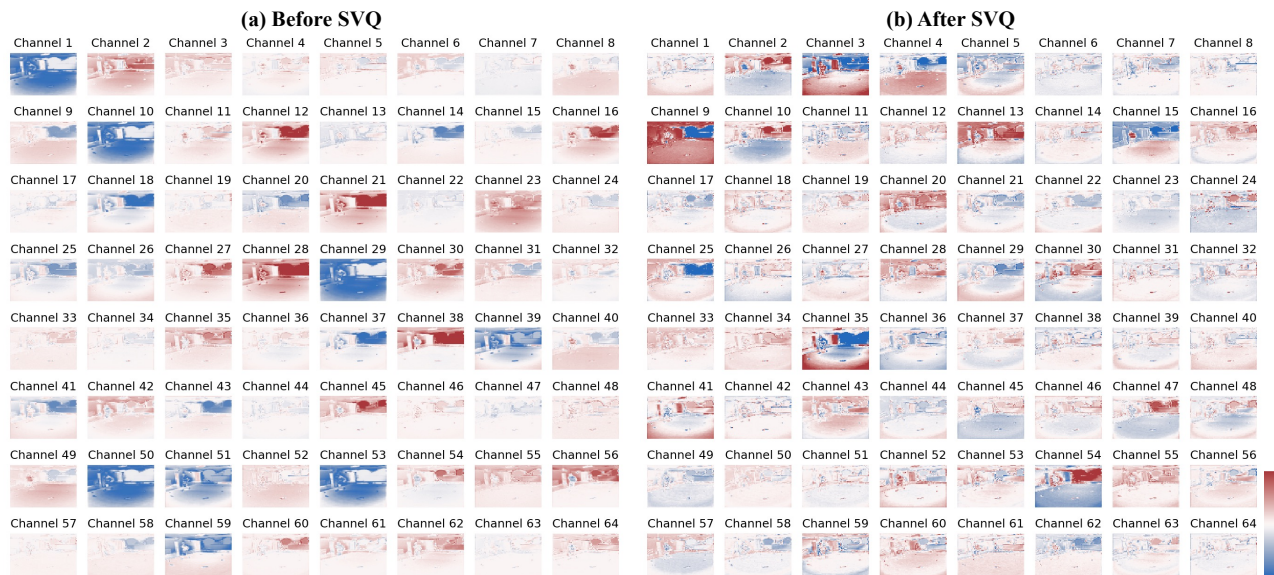


Figure 14. Latent feature map on the Human3.6M dataset: (a) feature map before SVQ, and (b) feature map after SVQ.

D. Additional qualitative results

D.1. Forecasting errors on WeatherBench and TaxiBJ datasets

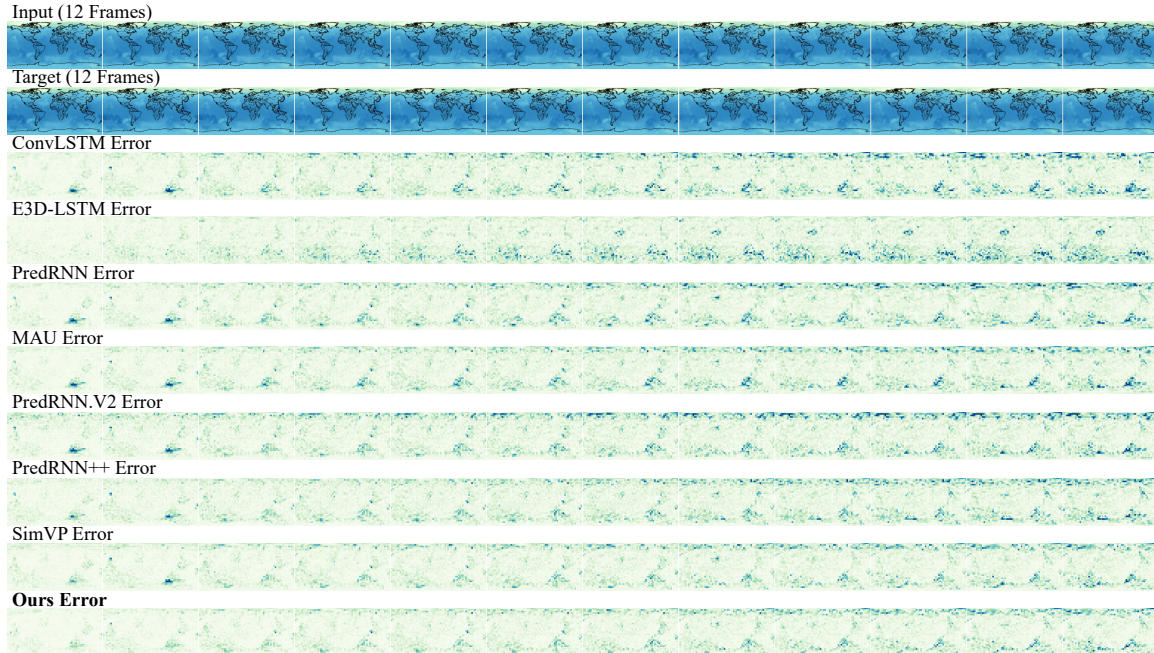


Figure 15. The qualitative forecasting errors on WeatherBench-S temperature dataset.

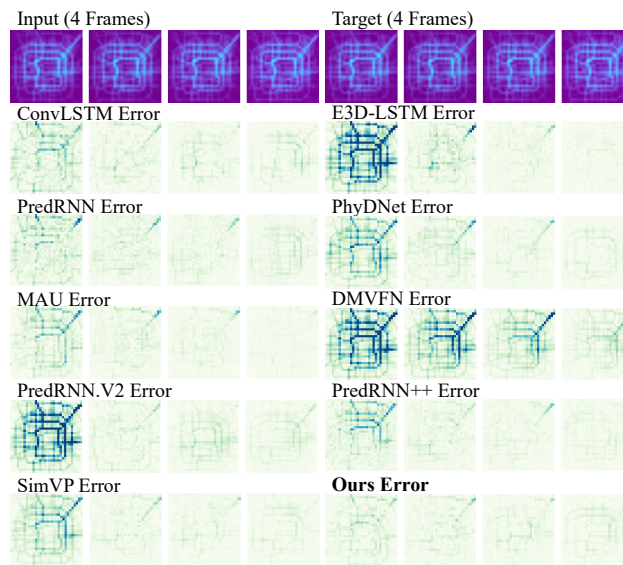


Figure 16. The qualitative forecasting errors on TaxiBJ dataset.

D.2. Additional forecasting samples

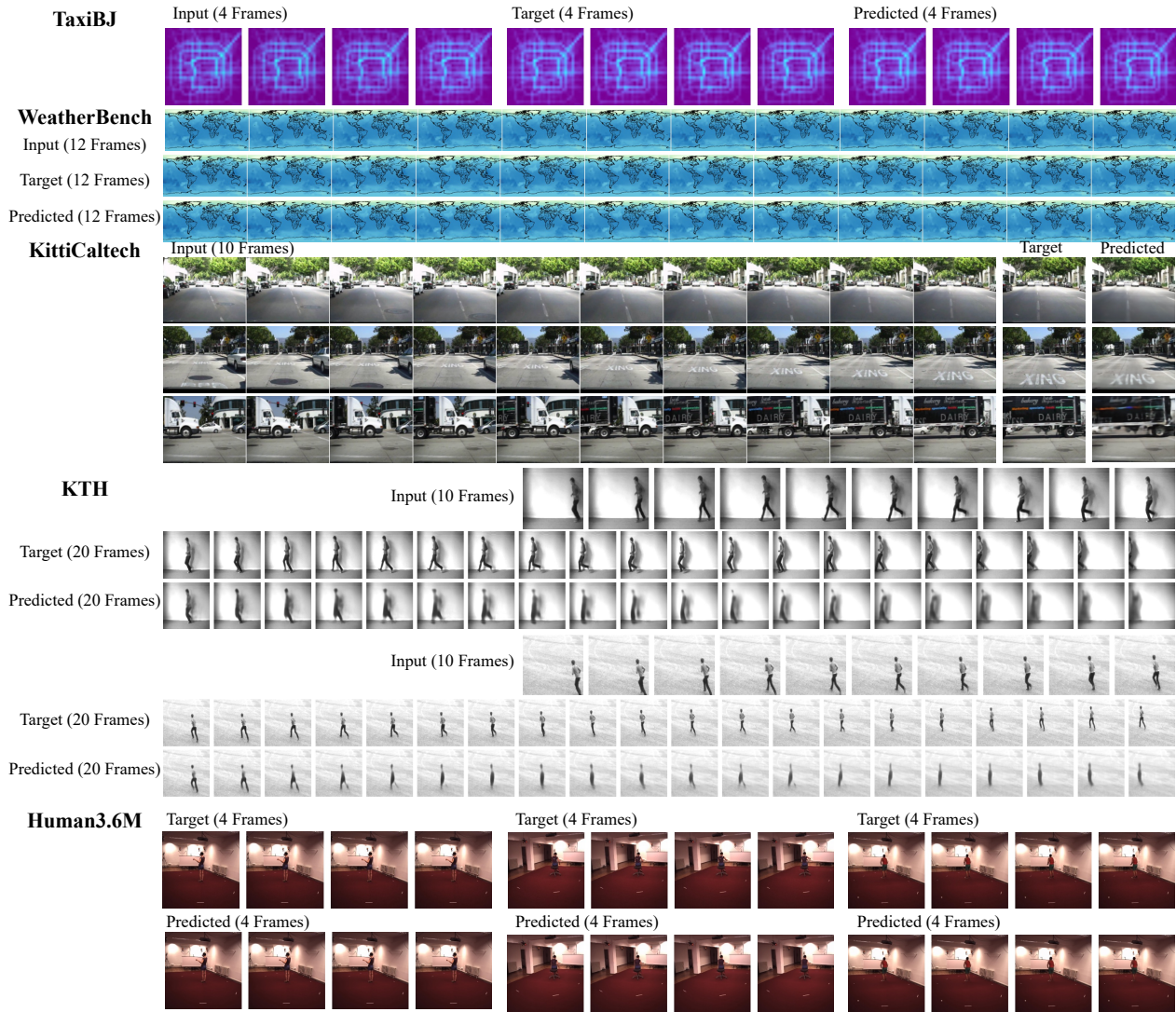


Figure 17. Forecasting samples of SimVP+SVQ model on the test set of TaxiBJ (32×32), WeatherBench (64×32), KittiCaltech (160×128), KTH (128×128), and Human3.6M (256×256). Zoom in for details. Our model produces accurate predicted frames for different tasks.